NUREG/CR-0934
SAND79-0938
R7

MOLTEN SODIUM INTERACTIONS WITH BASALT CONCRETE AND SILICEOUS FIREBRICK

R. U. Acton, R. A. Sallach, J. E. Smaardyk, L. A. Kent

Printed August 1979

Sandia Laboratories

SF 2900 Q(7-73)

Prepared for
U. S. NUCLEAR REGULATORY COMMISSION

NOTICE

This report was prepared as an account of work sponsored by an agency of the United States Government. Neither the United States Government nor any agency thereof, or any of their employees, makes any warranty, expressed or implied, or assumes any legal liability or responsibility for any third party's use, or the results of such use, of any information, apparatus, product or process disclosed in this report, or represents that its use by such third party would not infringe privately owned rights.

The views expressed in this report are not necessarily those of the U. S. Nuclear Regulatory Commission.

Available from
National Technical Information Service
Springfield, VA 22161

NUREG/CR-0934
SAND79-0938
R7

MOLTEN SODIUM INTERACTIONS WITH BASALT CONCRETE AND SILICEOUS FIREBRICK

R. U. Acton
R. A. Sallach
J. E. Smaardyk
L. A. Kent

Date Published: August 1979

Sandia Laboratories
Albuquerque, NM 87185
operated by
Sandia Corporation
for the
U. S. Department of Energy

Prepared for
Division of Reactor Safety Research
Office of Nuclear Regulatory Research
U. S. Nuclear Regulatory Commission
Washington, DC 20555
Under Interagency Agreement DOE [illegible]50-75
NRC FIN No. A1016

Abstract

The interactions of molten sodium with fast reactor construction materials are being investigated for safety analysis purposes. Basalt concrete has been used in the floor of the containment building under the reactor vessel in certain reactor designs. In these designs, the basalt concrete is protected by a steel liner and several courses of firebricks.

Molten sodium was poured into large basalt concrete crucibles. For one test, the cavity of the concrete crucible was unprotected. In another test, the cavity was covered with two layers of firebricks and a steel insert. The third test also used firebricks and a steel insert, however, the cavity sidewalls were excluded from the test in an effort to present the cavity bottom with a one-dimensional sodium attack. In the latter two tests, the steel insert was intentionally flawed so that the sodium might come in contact with the firebricks and the concrete. In all three of these tests, vigorous exothermic reactions were observed between the sodium and the concrete and between the sodium and the firebricks. The reactions continued until all of the sodium had been consumed. The three basalt concrete crucibles cracked severely.

Acknowledgments

The authors would like to acknowledge the help and guidance of R. L. Coats and N. R. Keltner of Sandia Laboratories and of M. Silberberg and T. Walker of the Nuclear Regulatory Commission. Special thanks are due to Paul Adams for the strain gauge instrumentation and analysis. Finally, we express our appreciation to C. Whitney and J. Ross without whose help the tests would not have been run.

Contents

Illustrations

Introduction

In order to characterize and model the reactions of molten sodium with nuclear reactor construction materials, a series of large scale interaction experiments has been conducted. Three of these experiments have been performed on basalt concrete. The experiments performed involved heating a desired quantity of sodium (up to 250kg) in a stainless steel vessel and then dumping the sodium into the nitrogen inerted cavity of a basalt concrete crucible. Energetic exothermic reactions were observed in all three tests. The interactions between the molten sodium and the firebricks and between the sodium and the concrete proceeded as long as sodium was available. Other investigators have looked at these interactions, but few on a large scale.

The large-scale experiments are augmented by physical and chemical separate effects tests in which individual parameters and chemical reactions may be studied.

This work is sponsored by the U. S. Nuclear Regulatory Commission and is a part of the Commission's confirmatory research effort in the advanced reactor safety program.

Sodium Facility

The facility in which the sodium-concrete interaction experiments are performed is shown in Figure 1. Basically the system involves transferring sodium from commercially available 55 gallon drums into a stainless steel heating tank. After reaching the desired temperature, the sodium is gravity dumped into the concrete crucible which is housed inside a steel test chamber.

Sodium is purchased in steel drums which serve as the initial part of the charging system. Cylindrical drum heaters (~6kW) are used to melt the sodium in the drum. Transfer from the drum is accomplished by first evacuating the dump tank and then pressurizing the drum, using argon.

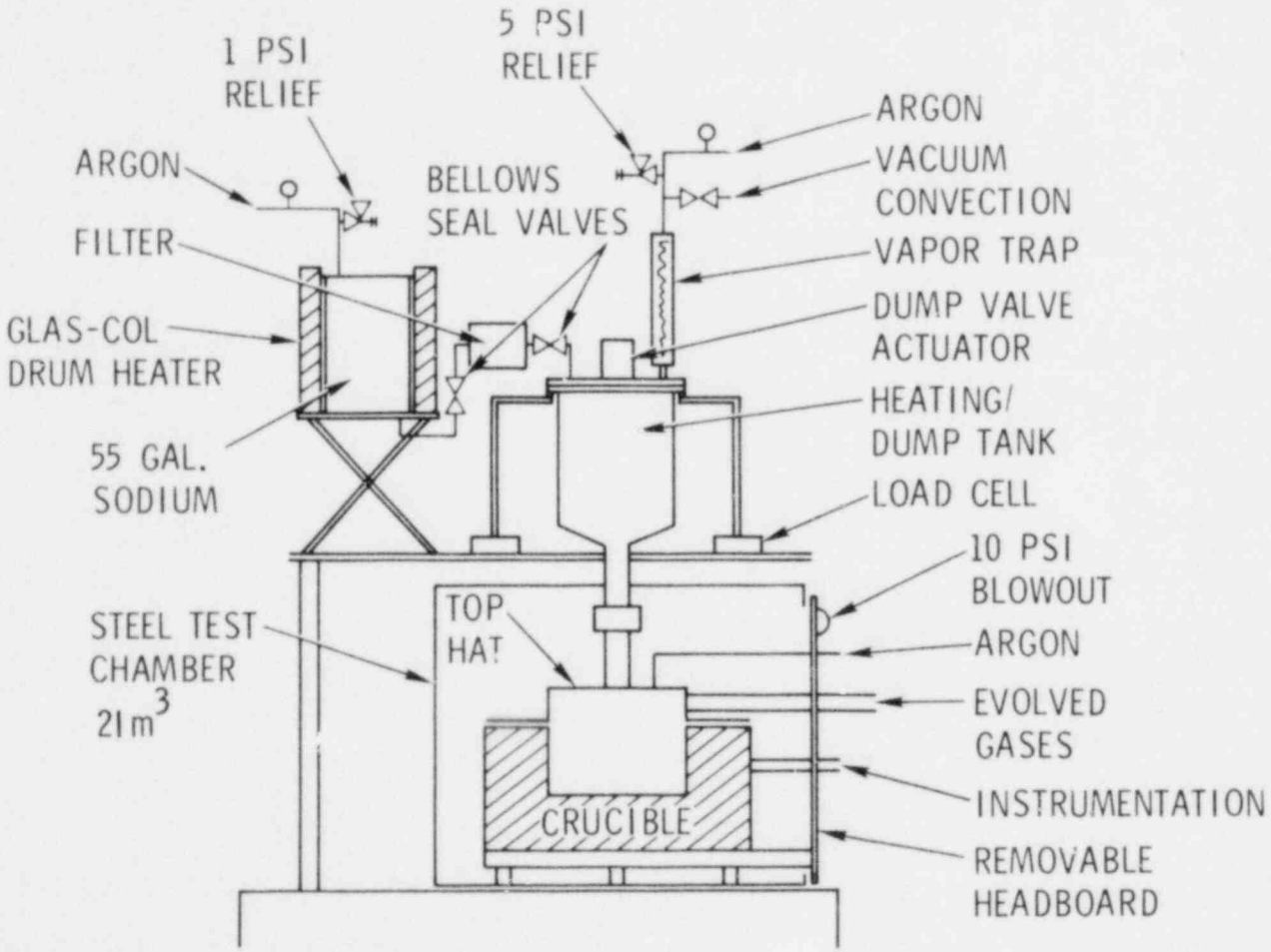

Figure 1. Sodium Facility

Trace heated stainless steel tubing is used as the transfer line. A sintered metal filter is incorporated into the transfer line.

The heating/dump tank is of 316 stainless steel construction. The ASME Boiler and Pressure Vessel Codes were specified in the tank's manufacture. The allowable stress for 316 stainless is 6.9 MPa at 1123K. A class 1 rating was specified which required radiographic inspection of all welds. The heaters used to heat the tank include sheathed tubular resistance heaters external to the tank as well as a sheathed immersion heater. The external heaters are controlled in three separate zones. Thermocouple feedback from each zone is used in conjunction with three-mode temperature controllers which, in turn, control the power delivered from a distributed-zero, crossover power controller. These controls make it possible to maintain a uniform tank temperature, alleviating thermal stress problems. A large vapor trap is incorporated into the tank to obtain pressure relief from the thermal expansion of the molten sodium. The valving mechanism used for dumping the sodium is a combination conical valve and seat with a stainless steel rupture diaphragm. The valve is pneumatically actuated.

The facility is isolated with no other personnel or buildings within a one kilometer radius. Residue from the tests is placed in shallow pits and watered down using accepted disposal methods.

Instrumentation

The instrumentation used for the large-scale sodium-concrete interaction experiments can be divided into three areas: 1) the overall data acquisition system, 2) gas analysis and 3) concrete penetration measurements. The crucible instrumentation is shown in Figure 2. Temperature, pressure, gas flow and moisture sensors were used as a part of each test. Strain gauges were used on the steel insert of test 2. The penetration of the sodium-concrete reaction zone into the concrete was monitored by an ultrasonic pulse-echo technique.

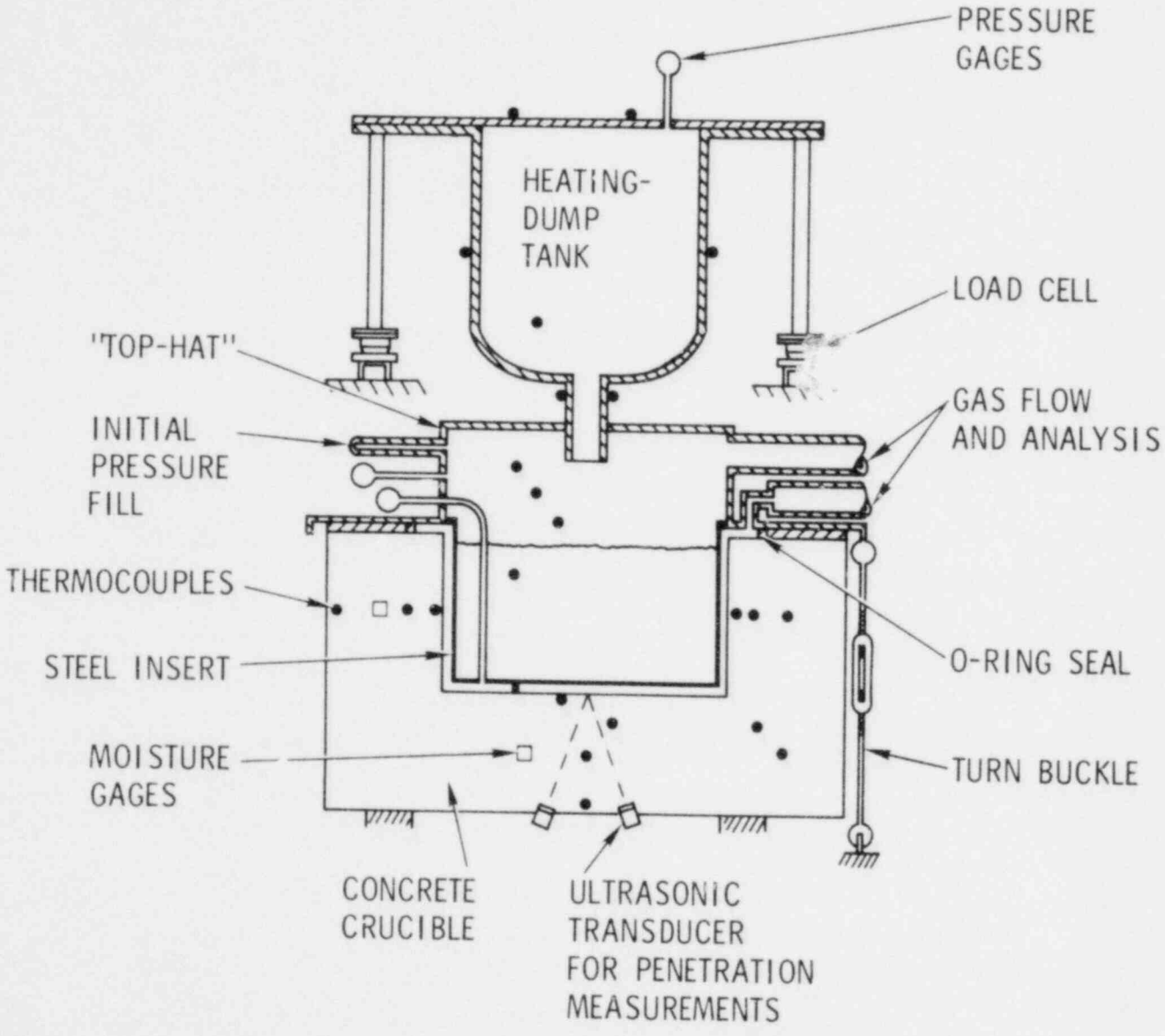

Figure 2. Location of Instrumentation for Basalt Concrete-Sodium Experiment
(Drawing depicts a crucible with a steel insert but without firebricks.)

Data Acquisition

The data acquisition system is a facilities installation and serves the sodium-concrete work as well as several other reactor safety programs (molten core and fragmentation). The system is shown schematically in Figure 3. The software was developed to use a modular technique. Only part of the operating test program is in core at any one time. A psuedo operating system loads files from tape and then transfers control to the file program. The program executes and turns control back to the operating system. Prior to a test an initialization program sets up calibration and specifications for each data channel. The data acquisition program is interactive so that parameters may be changed as a test progresses. A small amount of data reduction is performed during the test to aid in decision making.

Gas Analysis

Two chemical aspects of the sodium-concrete interaction are monitored during the tests, both related to the gas evolved during the interaction. The first is the identification of the gaseous species which are being evolved and the second is the measurement of the rate of gas evolution.

The identities of the gaseous species are determined by mass spectrometry with a quadrupole mass spectrometer. The instrument has a selectable mass range of 0-200 atomic mass units (AMU). Often called a residual gas analyzer, the instrument is most suited for the identification of the permanent gases such as H_2, CO, CO_2, N_2, O_2, etc. Composition can be determined if the necessary peak-height/partial-pressure calibration curves are known.

Since the maximum operating pressure in the mass spectrometer is $\sim 10^{-3}$ N/m^2 (1.4×10^{-6} torr), sampling of the evolved gases proceeds through three pressure reduction stages. A small part of the exhaust gases is withdrawn from the exhaust or vent pipe that leaves the "tophat" and passed through a glass wool filter to remove particulate matter. In turn, this filtered gas stream is sampled by another pumping system from which the final sampling is accomplished by the mass spectrometer vacuum

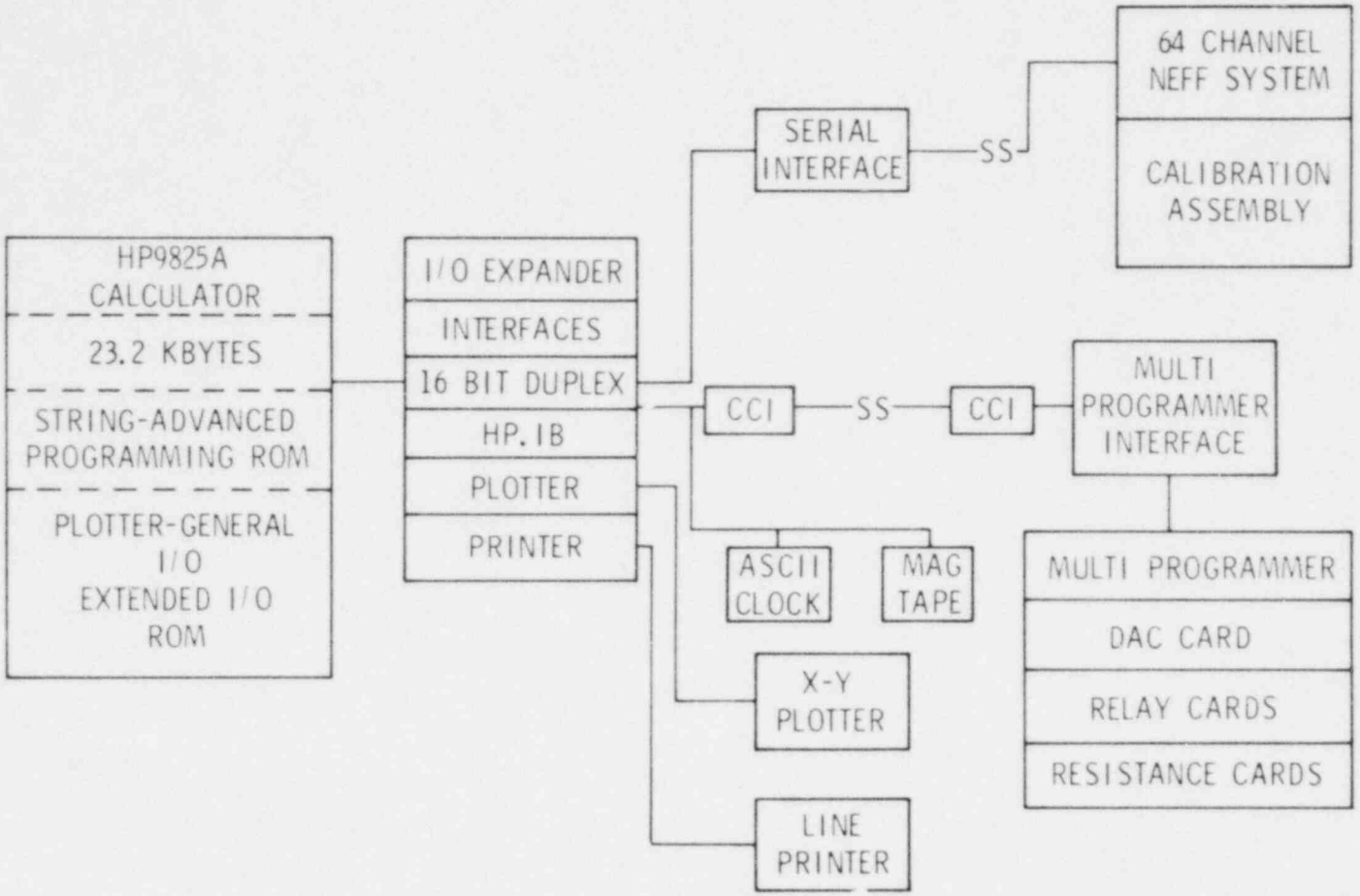

Figure 3. Diagram of Sodium Facility Data Acquisition System

system. Sufficient gas flows are maintained in the total sampling system so that the residence time is less than 15 seconds. During the tests, the mass spectrometer repeatedly scans between 0 and 48 AMU, taking about two minutes per scan.

The rate of gas evolution is measured by the pressure drop across a laminar flow element. The gases are conducted through a scrubber system in order to remove particulate matter. The flow element is placed downstream from the scrubber since it is easily plugged. A further advantage of this location is that the gas temperature has been brought to a nearly constant value, thus simplifying the calculation of flow rates. Apparent flow rates up to $5m^3$/min can be measured. The true flow rates may be calculated if composition is accurately known, assuming that the viscosity of a gas mixture is a linear combination of the viscosities of the component gases.

Concrete Penetration Measurements

The pulse-echo ultrasonic system used in these experiments is shown schematically in Figure 4. This system is identical to the one described in reference 1, and a detailed description of its operation is provided there. To summarize, the system measures the time required for an acoustic signal, generated by the transmitting transducer, to traverse the specimen, be reflected from the sodium-concrete interface, and return to the receiving transducer. When a measurement at some time, t, into the test is compared with a calibration measurement that was taken before the test, the distance the interface has moved during the intervening time is given by

$$\Delta\ell(\tau) = \frac{C(T)}{2}\left(\tau(0) - \tau(t)\right) \qquad (1)$$

where C(T) is the temperature-dependent acoustic wave velocity in the crucible material and Tau (τ) is the travel time of the acoustic wave. With temperature gradients in the concrete, this equation can be approximated by the series expansion

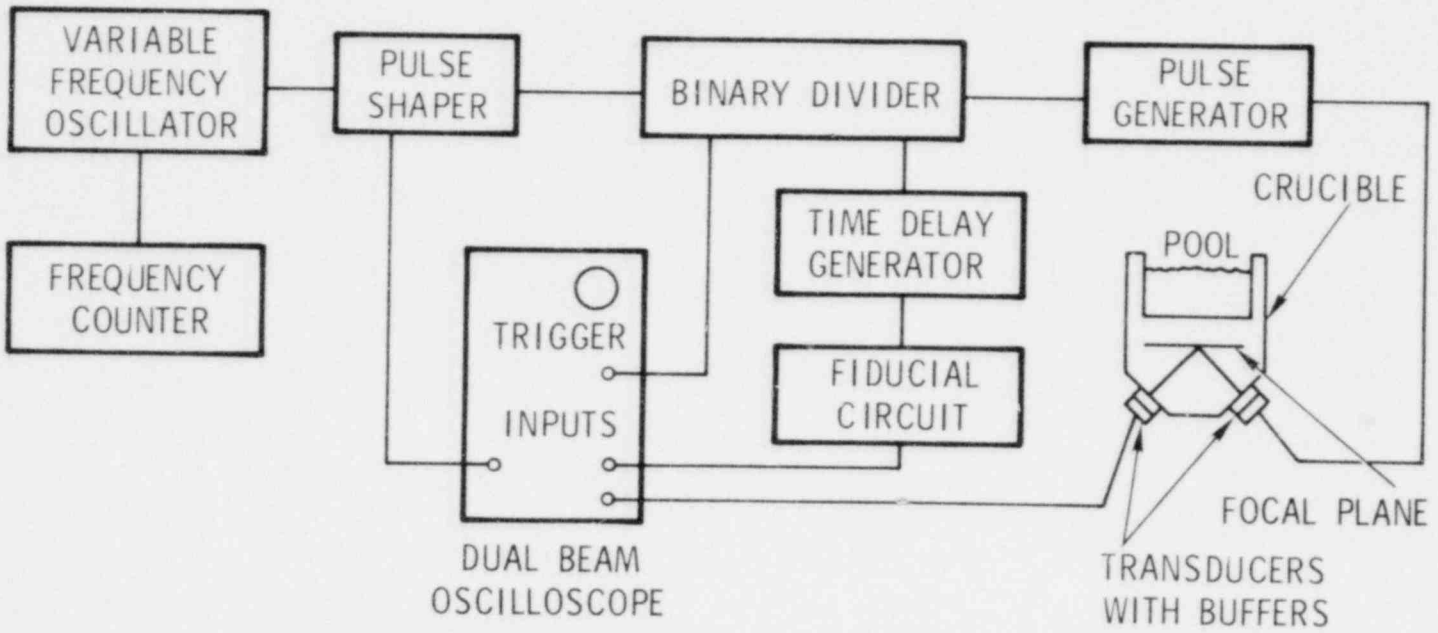

Figure 4. Instrumentation Schematic for Pulse-Echo Ultrasonic Technique of Concrete Penetration Measurements

$$\Delta\ell(t) = \frac{C_I}{2} - \left[\tau(0) - \tau(t) + 2 \sum_{i=1}^{N} \left(\frac{1}{C_i} - \frac{1}{C_0}\right) \ell_i(t)\right] \qquad (2)$$

where the temperature field in the concrete at time t is approximated by N uniform temperature zones, $\ell_i(t)$ is the thickness of the ith zone, C_i is the acoustic wave velocity in the ith zone, and C_0 is the reference acoustic velocity taken at room temperature, and C_I is the acoustic velocity taken at the hottest zone.

The mean acoustic wave velocity of basalt aggregate concrete is 5.64km/s at room temperature.[2] The velocity variation with temperature is shown in Figure 5.[3]

Strain Gauges

Weldable strain gauges were used on the steel insert of test 2 to see if the intentional flaw in the bottom plate might propagate because of the thermal shock of the sodium spill. The gauges consist of a short length of nickel-chromium alloy wire which has been etched so that a sensitive element is formed. The wire is insulated by highly compacted magnesium oxide powder and encased in a small diameter type 321 stainless steel tube. The tube is welded to an exterior metal flange which enables the gauge to be welded in place.

Normally the nickel-chromium gauge element is restricted for use to temperatures below 616K because the electrical resistivity of the element changes at higher temperatures. However, since these changes require a finite time to occur, it is feasible to use the gauge as high as 1090K in situations where the time of interest above 616K is a matter of minutes or less. Use of the nickel-chromium gauge is attractive since the change in electrical resistance due to temperature is about one-tenth that of platinum-tungsten or Nichrome V gauges. Strain gauges have been extensively characterized with respect to the effect of temperature, but only for constant or slowly changing temperatures. Since the temperature environment on the unheated side of the crucible

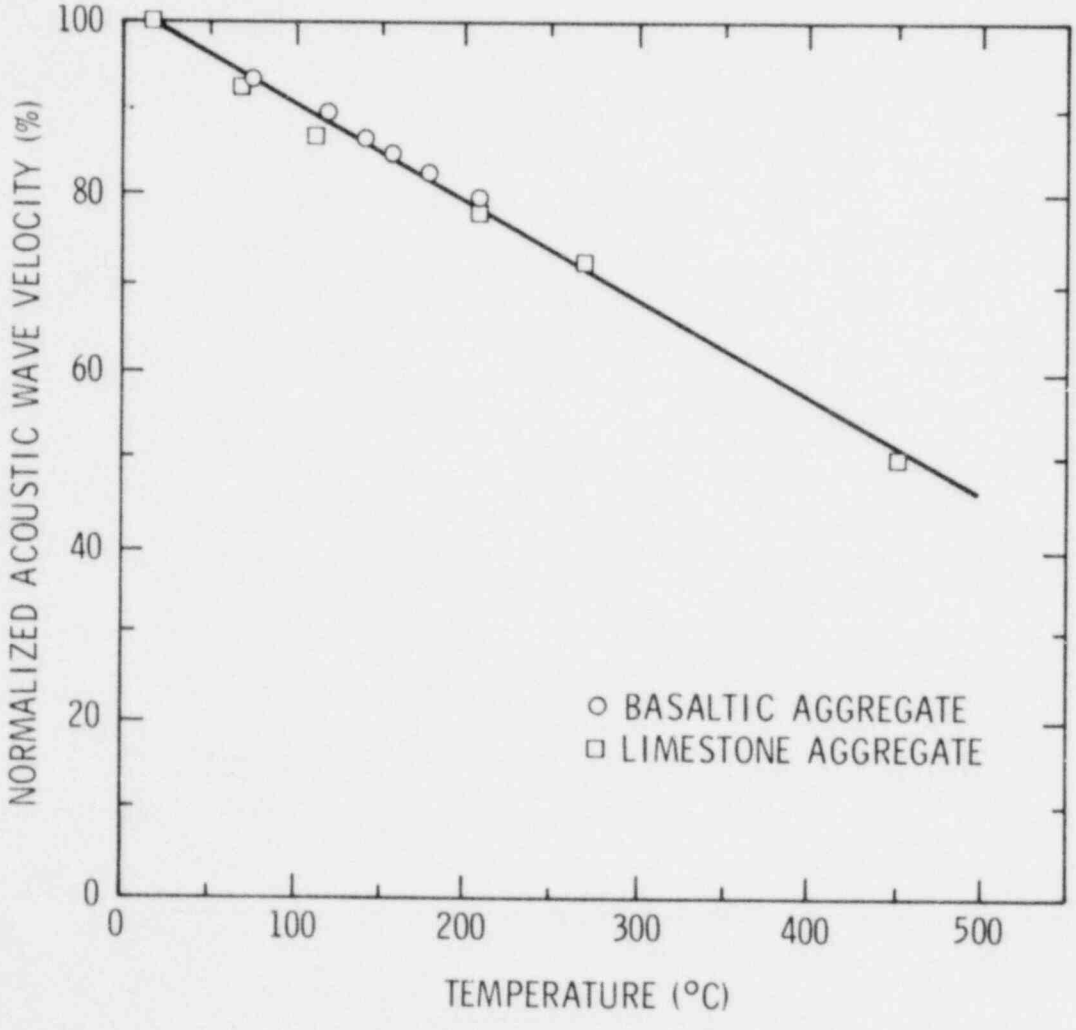

Figure 5. Acoustic Wave Velocity Variation in Concrete

insert was predicted to be characterized by a temperature increase of 55K/s, an investigation into the behavior of the strain gauges was initiated, see Appendix B.

Materials

Basalt Concrete

The concrete crucibles used in these experiments were cast using basalt sand and basalt aggregate obtained from the same source[4] that supplied materials for construction for the Fast Flux Test Facility (FFTF). Grain size distribution of the materials is shown in Figure 6. The mixing ratio for FFTF basalt concrete was obtained from the Hanford Engineering Development Laboratory (HEDL)[5] and is given in Table 1. The crucibles were cast, under contract, by the Eric H. Wang Civil Engineering Research Facility of the University of New Mexico. Test cylinders were cast at the same time as the crucibles and stored in 100% relative humidity. The cylinders were compression tested at standard intervals and on the day of a large scale test. Crucible construction is shown schematically in Figure 7. Crucibles were cast with a right circular cylindrical cavity. Cavity dimensions were varied to give different sodium contact area to sodium pool volume ratios. In all cases, crucible sidewall and bottom thickneses were 38.1 cm (15 in). All crucibles were cured at least 90 days before testing.

TABLE 1

Concrete Composition

	kg/m^3	%
Portland cement	269.1	11.4
Sand	844.2	35.8
Aggregate	1047.6	44.5
Water	149.0	6.3
Pozzalan	46.5	2.0

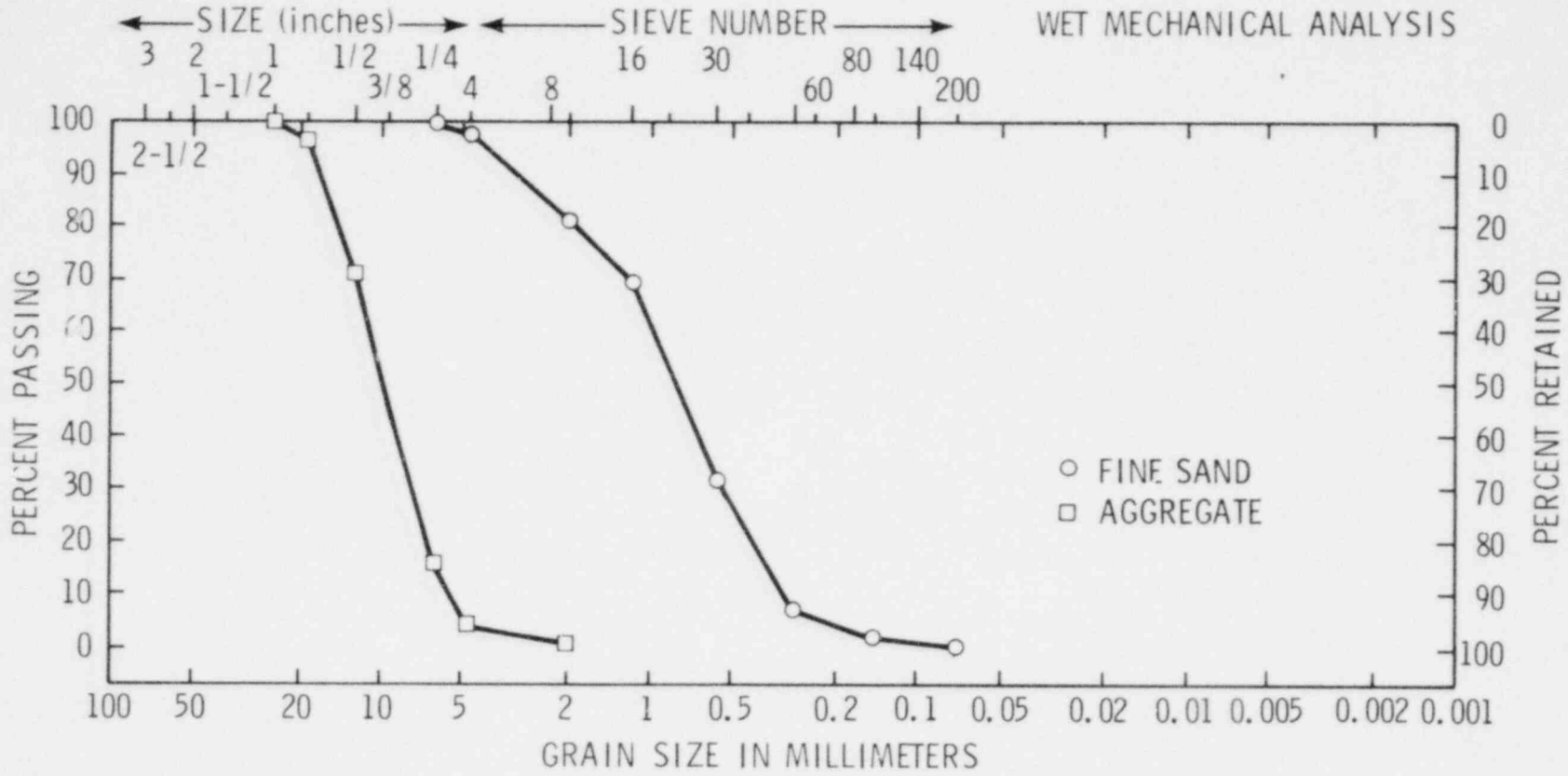

Figure 6. Basalt Sand and Aggregate Size Distribution Graph

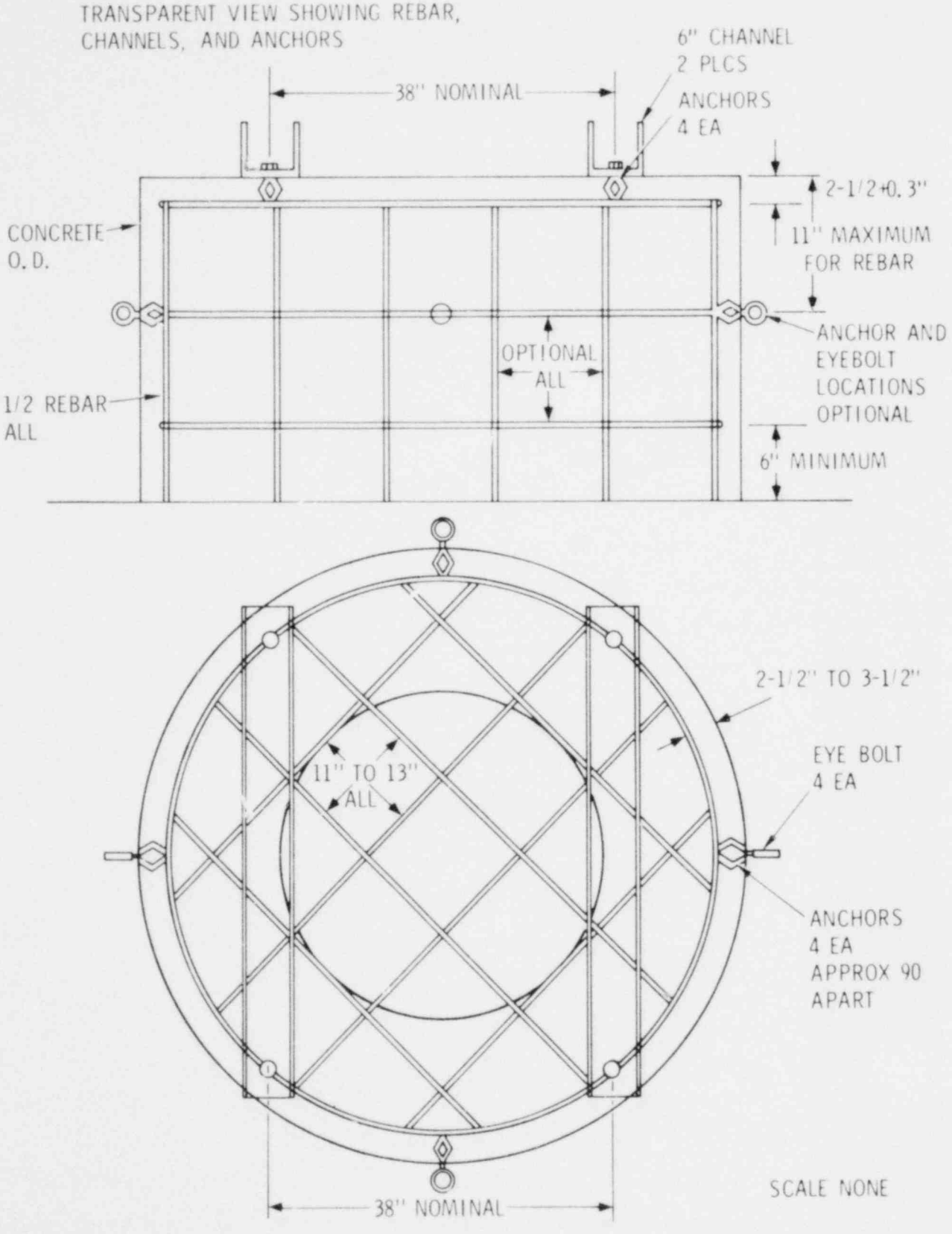

Figure 7. Concrete Crucibles Reinforcement

Firebrick

Two types of firebricks were used in these experiments, a dense firebrick and a light-weight insulating firebrick. FFTF cell hot liner design places the dense firebrick next to the steel liner and the insulating firebrick next to the concrete, see Figure 8. The dense firebrick has the trade name "Morex" and was supplied by Kaiser Refractories. The insulating firebrick is designated as G-20 and was supplied by A. P. Green Refractories. The composition of the firebricks is given in Table 2. Since both the basalt concrete and the firebrick compositon are over 50% SiO_2, their reaction with sodium was expected to be similar.

TABLE 2

Firebrick Composition

Oxide	Insulating	Dense
SiO_2	57-60%	56
Al_2O_3	33-36	38
Fe_2O_3	1-2	2
CaO	0.1-1.6	0.6
MgO	0.01-0.6	0.6
TiO_2	1.5-2.5	1
Alkalies	1-2	1.6
Bulk density	600-700kg/m^3	2130-2190

The refractory mortar used to cement the firebricks into the crucible was a commercial premixed product with t e trade name "Troweleze."

Experiments

The experiments are summarized in Table 3. In the first basalt concrete experiment, the bare crucible was exposed to a shallow sodium pool. In the second experiment, the crucible cavity was lined with firebricks and a steel insert (both sidewall and bottom), see Figure 9.

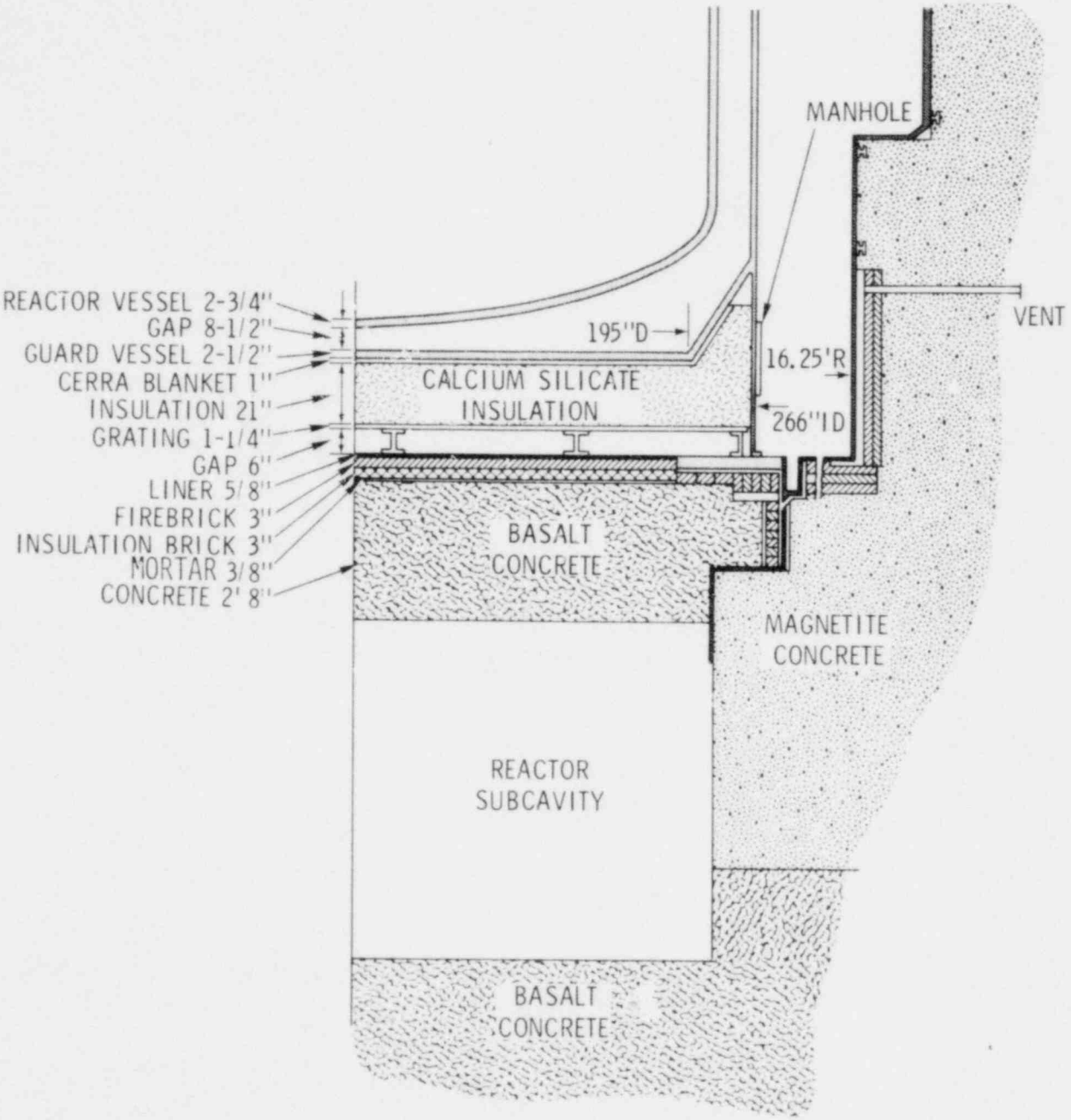

Figure 8. FFTF Reactor Cavity Structures

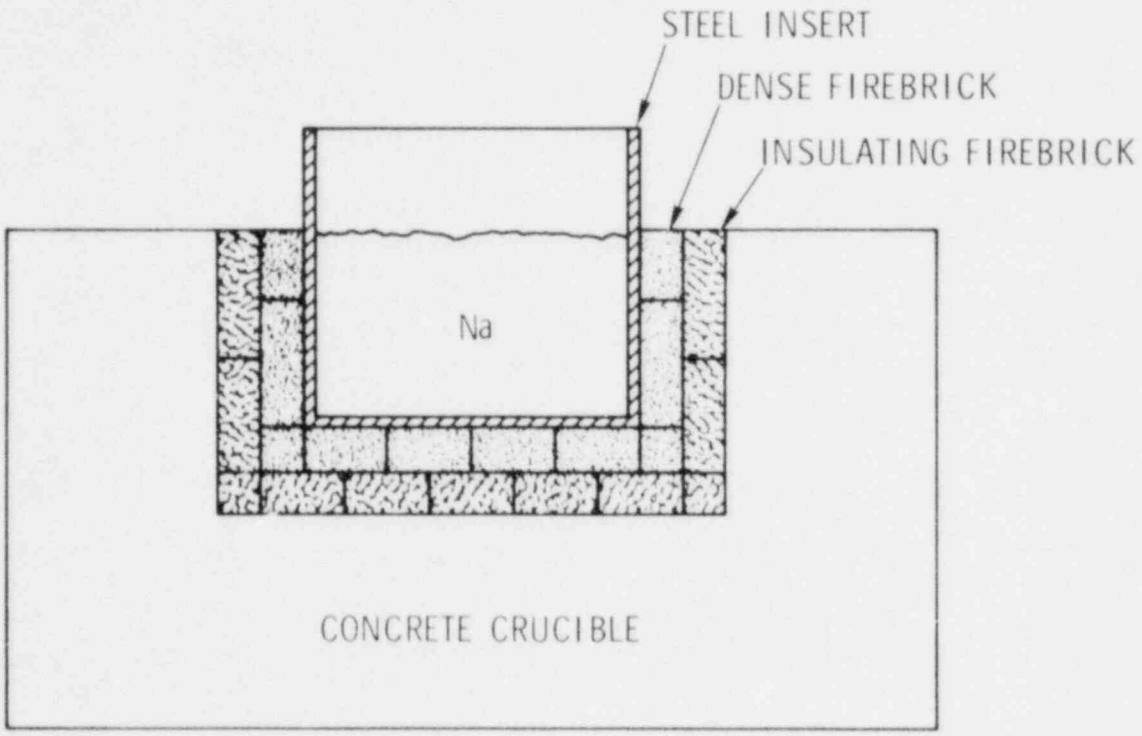

Figure 9. Arrangement of Firebrick and Insert in Concrete Crucible Cavity, Test 2 (Tophat and other test features are not shown.)

The cavity sidewall cracked radially in both tests. The third test was designed to exclude (as much as was possible with an already existing crucible) the sidewall from the interaction with sodium, Figure 10. For this test, firebricks were placed on the crucible cavity bottom but not on the sidewall. The steel insert was made such that a 2.5 cm annulus existed between the insert and the crucible cavity sidewall. This annulus was packed with magnesium oxide powder which is inert to sodium. The steel inserts of both the second and third tests contained an intentional flaw to simulate a defective liner that would allow the sodium to contact the firebrick and the concrete.

TABLE 3

Sodium-Basalt Concrete Experiments

	Test 1*	Test 2	Test 3
Crucible wt. kg	4090	3900	4000
Day of test comp. strength MPa	25.73	24.70	28.54
Cavity dia. cm	122	91	76
Cavity depth cm	30	51	71
Sodium wt. kg	128	68+45.5	239
Drop temp. K	873	873	973
Quench temp. K	700	620	700
Set-point K	823	823	823
Pool depth cm	13.2	30.5+20.2	76.8
Special features	none Bare cruci.	insert+fb.** 3-D	insert+fb. 1-D
Results:			
Energetic reaction	yes	yes	yes
Sodium consumed	all	all	all
Max. Erosion cm	6.4	all fb.	all fb.+ 30-35 cm of concrete

*Tests 1, 2, and 3 of this report were tests 11, 12, and 13 of the overall sodium-concrete program.

**fb. = firebricks

Test 1

128kg of sodium at 873K (600°C) were dumped into the bare cavity of the basalt concrete crucible. The resulting sodium pool was 13.2 cm

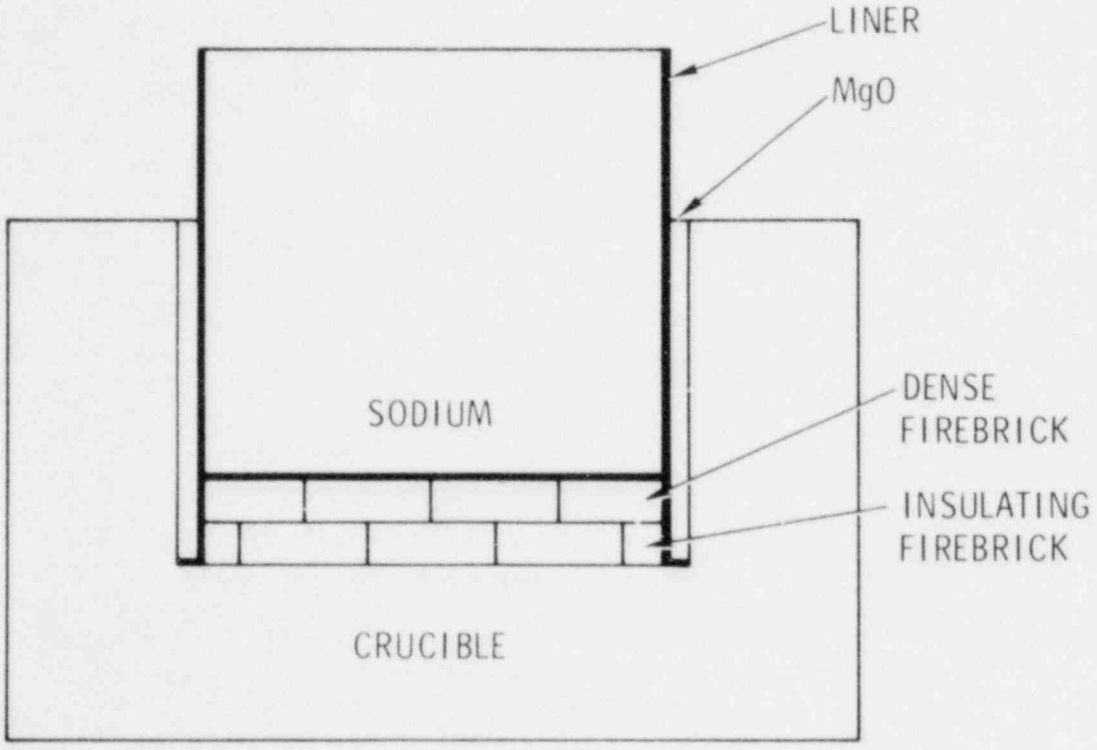

Figure 10. Experimental Arrangement of Liner, Firebricks and Magnesium Oxide Powder for Test 3

deep. The crucible cooled the sodium to 703K (430°C) before the pool heater could restore the pool temperature to a set-point of 823K (550°C), see Figure 11. The pool temperature remained at 823K for about 15 minutes before an exothermic reaction increased the pool temperature to 1043K (770°C). This reaction continued for about 75 minutes. At 280 minutes into the test, the pool heater failed terminating the test.

Posttest examination revealed that all of the sodium had reacted with the concrete leaving a cinder-like bed of reaction products. The products at one edge of the cavity burst into flame when exposed to the atmosphere. The crucible had numerous radial cracks extending completely through the cavity sidewall. The concrete had been preferentially attacked along these cracks due to enchanced water release. Figures 12 through 14 show the penetration and cracking of the crucible. The chemical analysis of two samples of reaction products is given in Table 4. One sample was obtained from the bottom of the crucible cavity near the center. The other sample was taken from the side of the cavity near the top. Substantial amounts of sodium hydroxide were found along with some sodium hydride. There was more hydroxide in the bottom sample, as would be expected from the hypothesized chemical reactions. (See section on Chemistry.) Other analyses (silica, alumina, etc.) were as expected from the concrete composition.

TABLE 4

Chemical Analyses of Reaction Products from Test 1

Constituent	Bottom/Center	Side/Top
$NaOH(+Na_2O)$	40%	18%
NaH	3	3
Na_2CO_3*	10	6
SiO_2	20	40
Al_2O_3	9	10
Fe_2O_3	9	10
CaO	9	13

*Probably from CO_2 in atmosphere reacting with NaOH of residue.

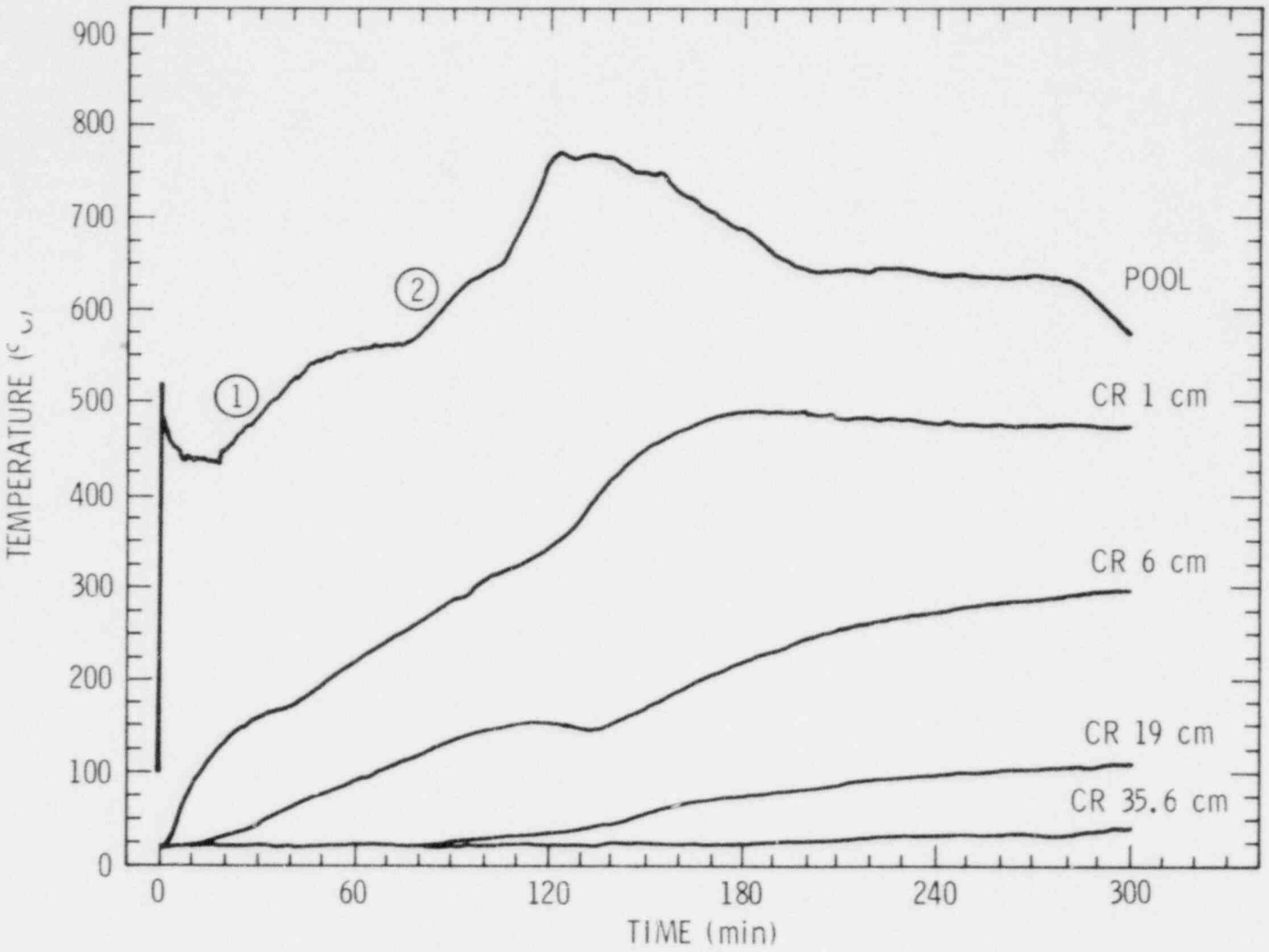

Figure 11. Crucible Temperatures and Pool Temperature, Test 1

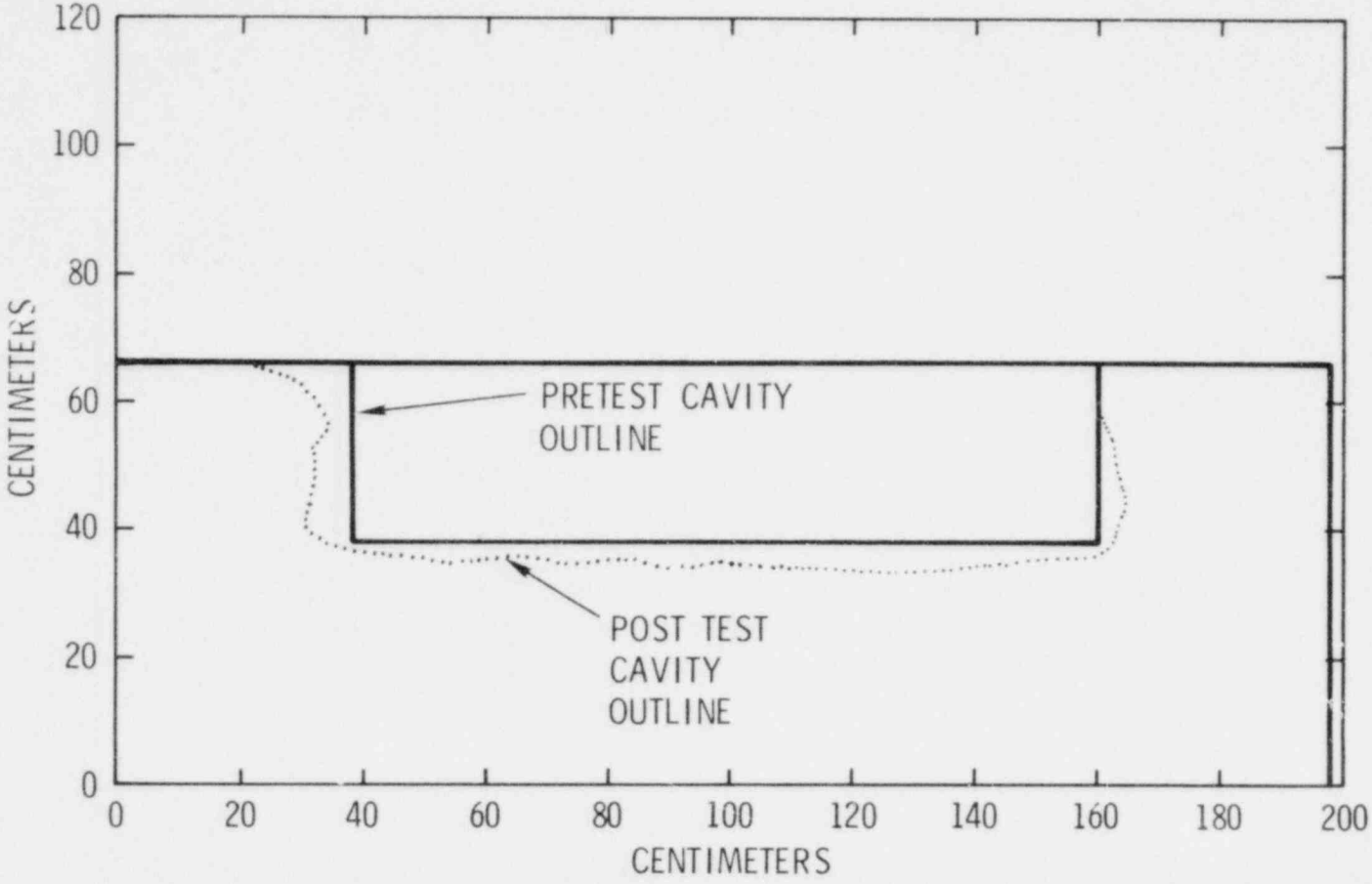

Figure 12. Basalt Concrete Crucible Penetration, Test 1

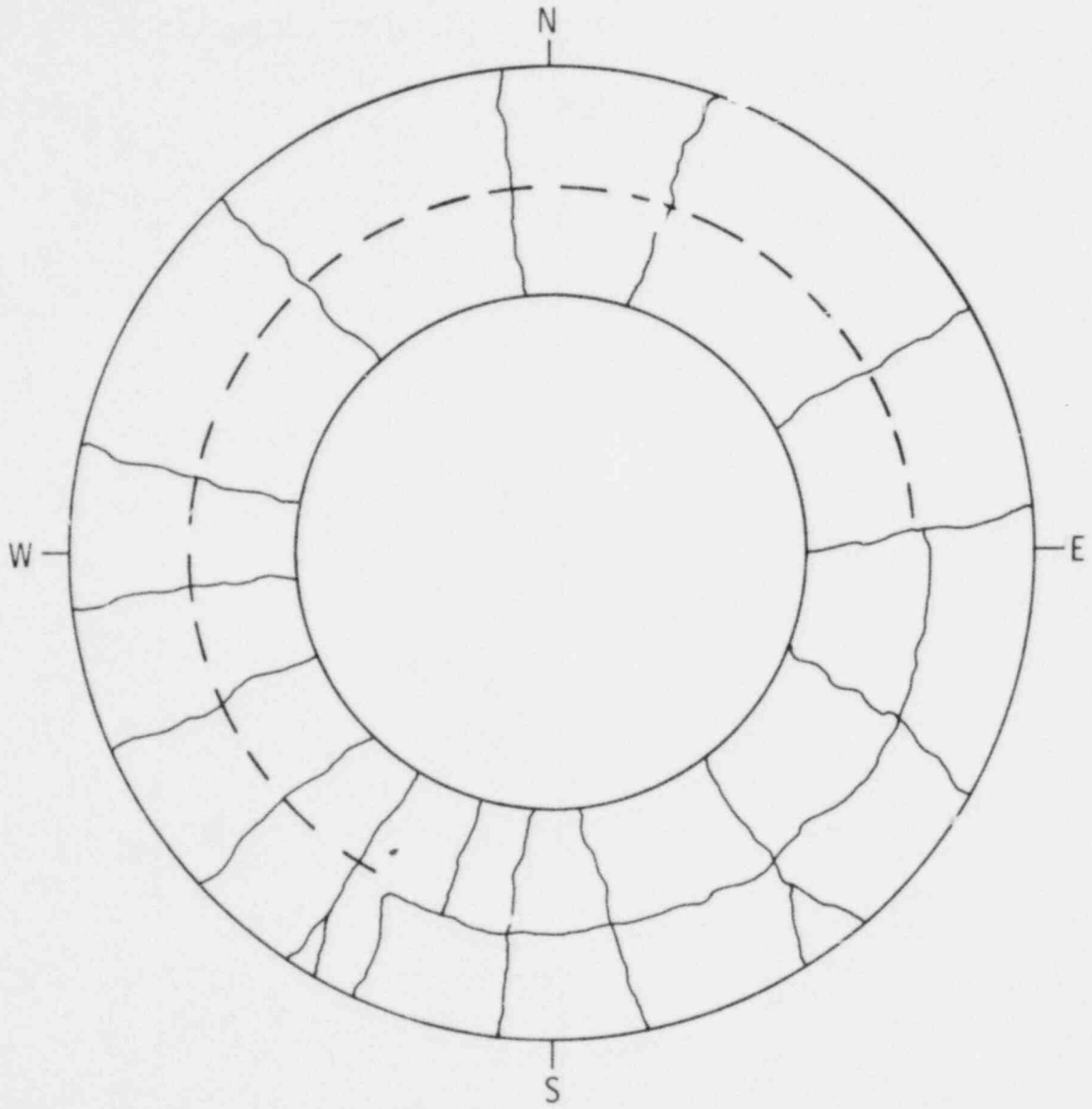

Figure 13. Crucible Crack Pattern, Test 1

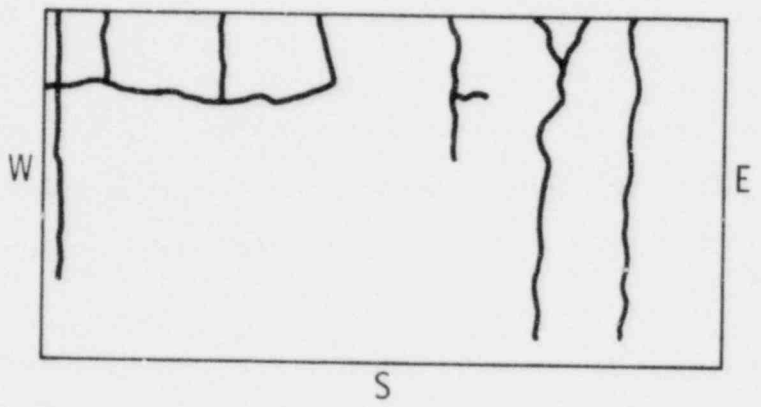

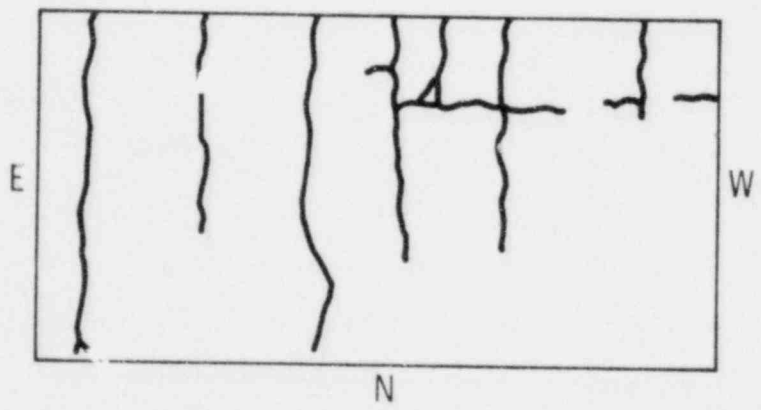

Figure 14. Side Views of Cracking Pattern of Basalt Concrete Crucible of Test 1

There are two nearly linear slopes on the heating portion of the pool temperature curve in Figure 11, labeled 1 and 2. The first slope occurred when the pool heater was bringing the pool temperature up to the set-point. The heater was operating at its maximum output of 30kW. Taking into consideration the mass of the sodium, this slope on the pool temperature curve corresponds to 10kW net heat input, indicating a heat loss (conduction, convection and radiation minus chemically generated heat) from the pool of 20kW. The second slope occurred when the heater had turned off (the temperature was over the set-point of 550°C). The heat being added to the pool could only come from exothermic chemical reactions. Slope one and slope two are nearly equal; therefore, assuming equal heat losses, the chemical reactions were contributing an additional 30kW during the time period of the second slope.

Test 2

The crucible cavity was lined with two layers of firebricks and a steel insert to simulate FFTF cell design, Figure 9. The steel insert was purposely flawed to simulate a defective liner that would allow the molten sodium to contact the firebricks and concrete. The simulated flaw in the bottom of the insert was instrumented with strain gauges to furnish data on the thermal stresses in the insert and possible flaw propagation. In addition to the normal crucible thermocouples, thermocouples were also placed between the insert and the dense firebrick, between the dense firebrick and the insulating firebrick and between the insulating firebrick and the concrete.

68kg of sodium at 873K (600°C) were dumped into the lined crucible cavity. The initial pool depth was 30.5 cm. Following initial cooling, the heaters restored the sodium pool temperature to 823K (550°C) and maintained it there for approximately 15 minutes. At that time, an exothermic reaction started in the first layer of firebrick (dense), Figure 15. Temperatures in this layer reached 1123K (850°C). A short

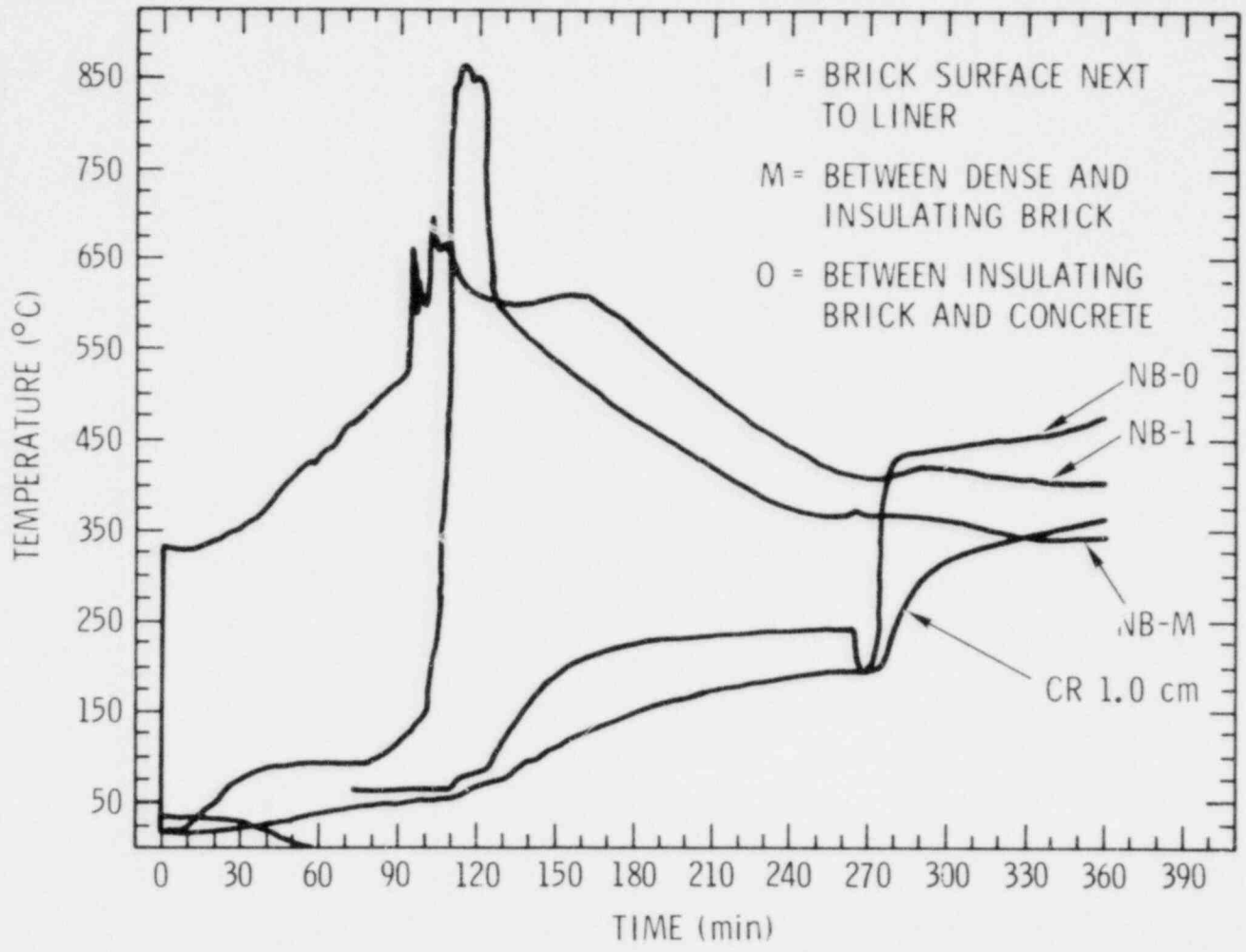

Figure 15. Test #2 North Brick (NB) Temperatures and Crucible (CR) Temperature (North Side)

time later, a temperature excursion was detected in the second layer of firebrick, followed by an excursion at the firebrick-concrete interface. Here, three hours into the test, the depth of the sodium pool had dropped about 20 cm as indicated by thermocouples. A sodium excess was desired for this test so a second sodium dump of 45.5kg was made. A large volume of gas vented from the test chamber when the second sodium dump was made--indicating that the concrete crucible was badly cracked at that time. In the eleventh hour of the test, an explosion occurred in the test chamber, presumably caused by hydrogen gas, terminating the test.

Posttest examination revealed that all of the sodium (113.5kg) had reacted. The reaction products from the sodium-firebrick reaction had bulged the bottom of the insert, in the direction of the cavity, about 4 cm--giving it the appearance of the bottom of an aerosol can, Figure 16. No radial distortion of the insert was noted. The upward force of the reaction products was strong enough to break two of the four turnbuckles that were used to hold and seal the tophat-insert assembly to the crucible. The concrete crucible was more severely cracked than was the bare crucible of test 1, Figure 17. Crack widths at the outer circumference were as much as 2.5 cm. Because this test was sodium limited, the sodium had not penetrated beyond the firebrick into the cracks as it did in test 1. The firebricks around the cavity sidewall had reacted with the sodium and changed color from light tan to a blue-black; however, the reacted firebricks retained their shape and position. The firebricks on the bottom underwent the same color change but could no longer be discerned as individual bricks. They had become a homogeneous mass that partially stuck to the bottom of the insert when it was removed.

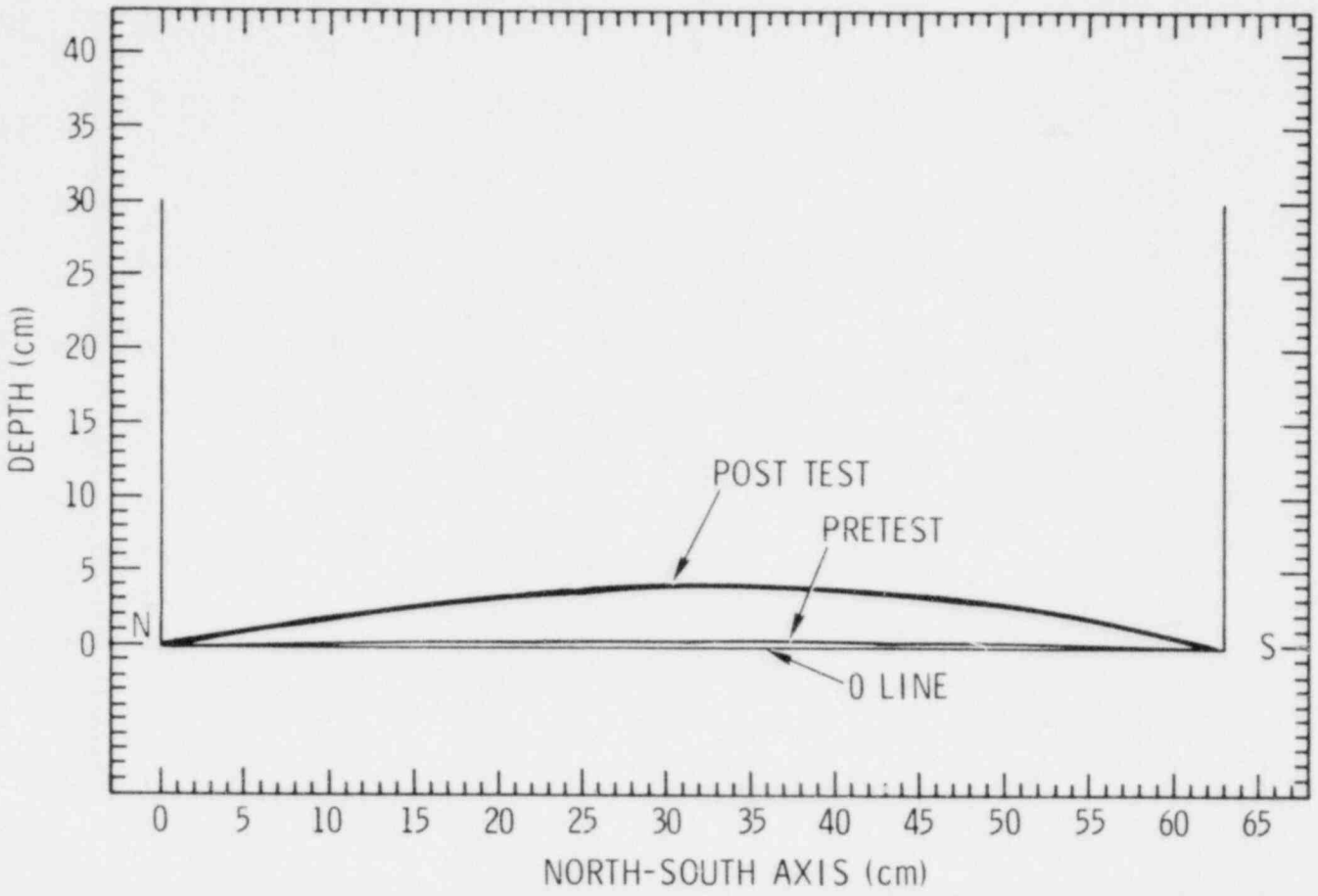

Figure 16. Test #2 Liner Configuration Posttest versus Pretest

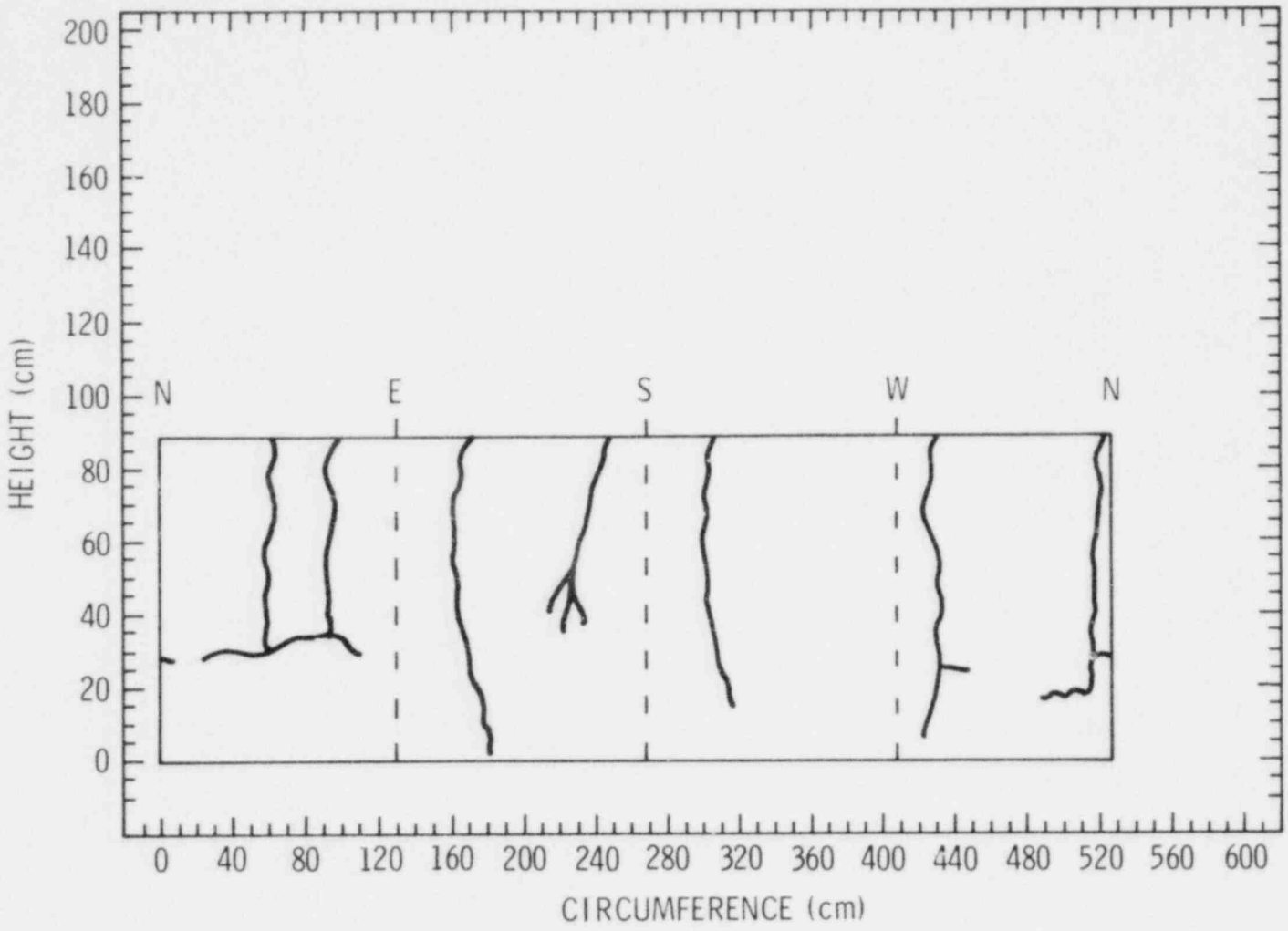

Figure 17. Test #2 Posttest Circumferential Distribution of Radial Cracks

Test 3

Test 3 was designed to provide for as nearly a one-dimensional test as was possible with an existing crucible. The design is shown in Figure 10. A steel insert was placed into the crucible cavity. The outside diameter of the insert was such that a 2.5 cm annulus existed between the insert and the crucible sidewall. This annulus was packed with magnesium oxide powder. MgO is inert to sodium. In this way, the effects of the sidewall of the concrete cavity were limited in the experiment. The bottom of the cavity was lined with two layers of firebricks as in test 2. The bottom plate of the insert was tack welded to the cylindrical sidewall of the insert just above the dense firebricks. The bottom plate contained a simulated flaw (15.2 x 0.64 cm) to allow the sodium to contact the firebrick.

239kg of sodium at 973K were dumped into the lined crucible cavity. The mass of the steel insert cooled the sodium to about 700K in 20 minutes. Immersion heaters brought the sodium pool temperature back to a set-point of 873K in 145 minutes. Thermocouples embedded in the firebricks and concrete monitored the progress of a reaction front through these materials. The sodium reacted with both layers of firebricks and the crucible bottom to a depth of about 25 cm. Figure 18 shows the reaction front progress. The pool immersion heater failed at 12 hours, ending the test.

Posttest examination revealed that the magnesium oxide powder was effective in keeping the molten sodium away from the cavity sidewall. The steel insert bottom plate, which had been tack welded at four points around its circumference, was pushed up into the cavity about 48 cm by reaction products. The pressure built up by these products was enormous, cracking the crucible horizontally at approximately the cavity floor level and opening these cracks as wide as 15 cm at the outer circumference of the crucible. All four turnbuckles that seal the tophat-insert to the crucible were broken. The sodium dump tank that sits on

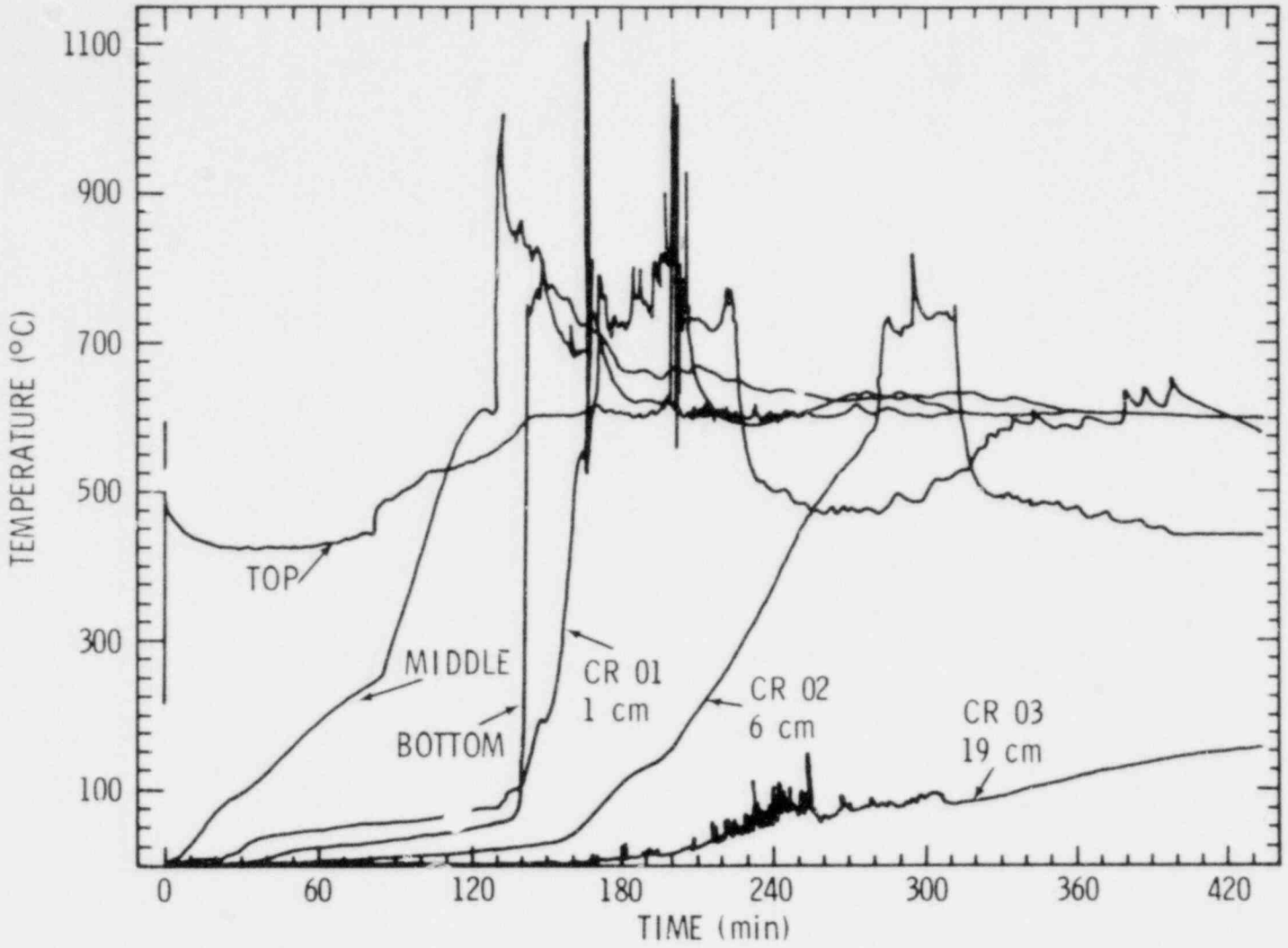

Figure 18. Firebrick and Crucible Temperatures, Test 3

top of the test chamber had been lifted 10 cm. Reaction products filled the cavity and were even found on top of the insert-bottom plate, see Figure 19. All of the firebricks in both layers had reacted. The bottom of the crucible had reacted to a depth of 25 cm, leaving a black, porous, cinder-like reaction product. The remaining 13 cm of concrete in the crucible bottom, although retaining the appearance of concrete, had little strength as it could be picked apart with a screwdriver. In another area of the crucible bottom, reaction products were found on the floor of the test chamber under the crucible--indicating total penetration of the 38 cm of concrete. However, the last part of this total penetration was along a crack.

Samples for chemical analyses were taken from several locations within the reaction product mass. The sample locations and descriptions are shown in Figure 19. The results of the analyses are given in Table 5.

TABLE 5

Analyses of Reaction Products - Test 3

	Sample			
	A	B	C	D
% Water soluble	58	76	47	44
NaH	21	0	3	3
$NaAlO_2$*	3	4	3	3
Na_2SiO_3*	8	23	21	21
NaOH	19	40	--	--
Na_2O	--	--	20	21
Undetermined	7	9	0	(3)
% Water insoluble	42	24	53	56
Al_2O_3	12	2	5	6
SiO_2	17	8	24	25
Fe_2O_3	1	4	6	5
CaO	1	4	8	9
Na_2O	6	1	6	7
Undetermined	5	5	4	4

*Identified by x-ray diffraction

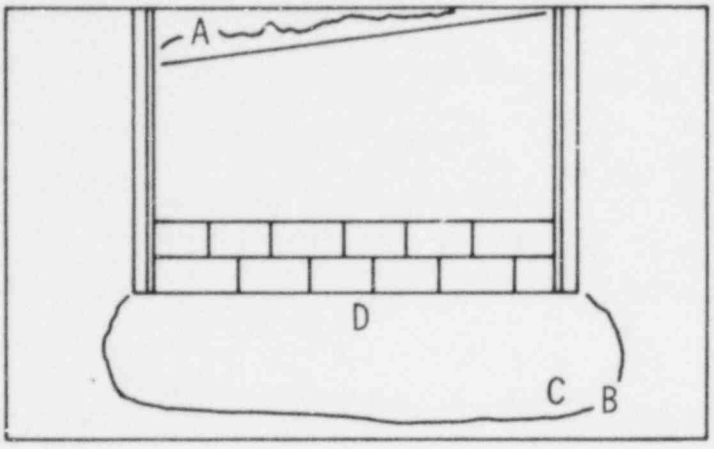

SAMPLE A: SLAG-LIKE MATTER TAKEN FROM TOP OF DISPLACED FLAWED-PLATE (INSERT BOTTOM PLATE)

SAMPLE B: YELLOWISH MATTER (ATTACKING PHASE) FROM SE PART OF CRUCIBLE

SAMPLE C: BLACK MATTER IMMEDIATELY BEHIND SAMPLE B

SAMPLE D: REACTED CONCRETE TAKEN JUST BELOW WHAT HAD BEEN BRICK-CONCRETE INTERFACE

Figure 19. Description and Location of Test #3 Samples for Chemical Analyses

Results

Chemical Results

Comprehensive, detailed chemical analyses were made on material from tests 1 and 3. These analyses included x-ray diffraction work to identify reaction products and standard determinations on water soluble and water insoluble fractions. The reaction zone of test 2 did not extend beyond the firebricks. Therefore only the reacted bricks were sampled, and these samples were only subjected to x-ray diffraction analysis.

From test 1, samples of the reaction products were obtained from two locations, as explained earlier. Substantial amounts of sodium hydroxide were found in both samples. A greater amount of sodium hydroxide was found in the sample from the bottom of the cavity near the center than in the sample from near the top edge. This is to be expected from the greater density of the hydroxide over sodium metal. Any sodium hydroxide formed on a vertical surface would drain downward. Its fluidity would decrease as sodium silicates are formed. The complete analytical results were given in Table 4. The x-ray diffraction results indicate that the major phases are sodium meta-silicate, Na_2SiO_3, and sodium hydroxide, NaOH. Other sodium silicates were not identified.

The reacted firebricks of test 2 were examined by x-ray diffraction. These bricks are largely silica and alumina and the identified reaction products were sodium meta-silicate, Na_2SiO_3, sodium aluminate, $NaAlO_2$, and sodium hydroxide, as expected.

Test 3 showed extensive reactions, forming a large volume of products. Samples were taken from four different locations as described earlier. The locations are shown in Figure 19. The locations were chosen in anticipation that further information on the chemical processes would be obtained. For this reason, extra care and effort were taken in their analyses.

Sample A was taken from the top side of the flawed bottom plate which had been pushed far up into the cavity sample. Presumably the sample is typical of the material that lay next to the sodium metal. Sample B was a yellowish material adjacent to the dehydrated concrete and thus may be representative of the material that reacts with (attacks) the concrete. At this particular location, the yellowish material was 3 cm thick, and a representative sample was easily obtained. Usually, this layer is less than 0.5 cm thick and obtaining a representative sample was difficlt. Sample C was taken from the reacted matter just above sample B. Sample D was taken just below what had been the original brick-concrete interface. Both samples C and D had a black, porous appearance. Since samples C and D are reacted concrete but located at different distances from the reaction front, it was anticipated that compositional differences might be observed that would be indicative of the diffusion processes occurring in the reacted matter, thereby aiding the interpretation of the chemical processes.

The analytical results are shown in Table 5. Sample A had a strikingly high amount of sodium hydride. At the temperatures of this test, sodium hydride would not have been expected to form or would have been expected to decompose. To account for its presence, it must be assumed that hydrogen gas release is inhibited so that local hydrogen gas pressures are above the decomposition pressure of sodium hydride. Sample B had a very high percentage of sodium hydroxide. The x-ray diffraction data indicate that sodium meta-silicate is a major compound; this is consistent with the large percentage of water soluble silicate, as more complex silicates are not readily water soluble. No sodium hydride was detected. Compositional differences were expected between samples C and D, but none were found. Both had small amounts of sodium hydride. Since water reacts with sodium hydride in a manner similar to sodium, the implication is that all water is consumed at or near the concrete interface and that the diffusion of sodium or its

equivalent in a thermodynamic sense) proceeds from the sodium pool through the reaction products to the same interface. The similarity of samples C and D suggests that the diffusion of the sodium may be fast relative to the diffusion of the water in the concrete.

Gas Flow

Hydrogen is the only permanent gas that has been detected in these tests on basalt concrete (with or without firebrick). This is as expected since neither the concrete nor the firebrick contain materials that would produce other gases. In addition, molten sodium is an efficient scavenger of many gases such as CO, CO_2, and O_2. These data do not preclude the presence of other vapor species in the atmosphere above the sodium pool. Sodium vapor is likely to be present, especially when the reaction temperatures exceed 973K. At higher temperatures, sodium oxide vapor is another possibility. However, these species rapidly condense as the gas temperature is lowered and would be removed by the sampling system.

Apparent gas flow rates from these tests follow a similar pattern: burst of gas as the sodium is dropped, with the flow building up to a broad maximum--then gradually decaying to low values. Secondary maxima in the flow can be observed at later times. Any interpretation of the later flow data is questionable because of the cracking of the concrete crucibles. For these tests, there is no way of knowing how much of the hydrogen escaped through these cracks or when the cracks formed. That the hydrogen gas did escape is evidenced by explosions in the test chamber.

Initial flow rates were moderate in relation to the amount of sodium reacted. In test 1, the initial apparent rate peaked between 0.2 and $0.3 m^3$/min and gradually decayed. The average flow for the first 60 minutes of test 1 was about $0.15 m^3$/min. This is approximately $0.1 m^3$ of evolved hydrogen gas per square meter of sodium-concrete contact area per minute. Based on the fact that for each mole of

hydrogen evolved two moles of sodium have reacted, these values suggest that 12% of the sodium had reacted during that time. At the beginning of test 3, a large quantity of hydrogen gas evolved, dropping quickly to almost nothing. The decreasing evolution rate can be accounted for by the formation of a large amount of sodium hydride.

Steel Insert Strain

The location of the strain gauge instrumentation around the intentional flaw in the steel insert of test 2 is shown in Figure 20. The flaw measured 15.2 by 0.6 cm. Neither this flaw nor the flaw in the insert of test 3 showed any tendency to propagate. A plot of the early time temperatures and strains in the insert are shown in Figure 21. The plot shows that at first the bottom plate bows downward but then, between 4 and 8 seconds, bows upward. The mild steel inserts of tests 2 and 3 were 0.95 cm thick.

Concrete Penetration Rate

Concrete penetration data were obtained from the ultrasonic instrumentation for tests 1 and 3. In test 2, the sodium was consumed by the firebrick before the reaction front reached the concrete so there was no significant concrete penetration.

The penetration data for test 1 are shown in Figure 22. The attack begins some time between 60 and 70 minutes into the test and proceeds at a fairly uniform rate of about 0.5 millimeters per minute. The total penetration is 40mm which agrees well with posttest examination results. From these data, it appears that the sodium was depleted at about 150 minutes into the test and that the chemical attack of the concrete ceased.

Test 3 yielded good acoustic data for the first 280 minutes of the test. By that time, the acoustic coupling between the crucible and the transducer had degraded to the extent that meaningful data could no longer be obtained. The data are plotted in Figure 23. It can be seen that significant penetration began at about 145 minutes into the test

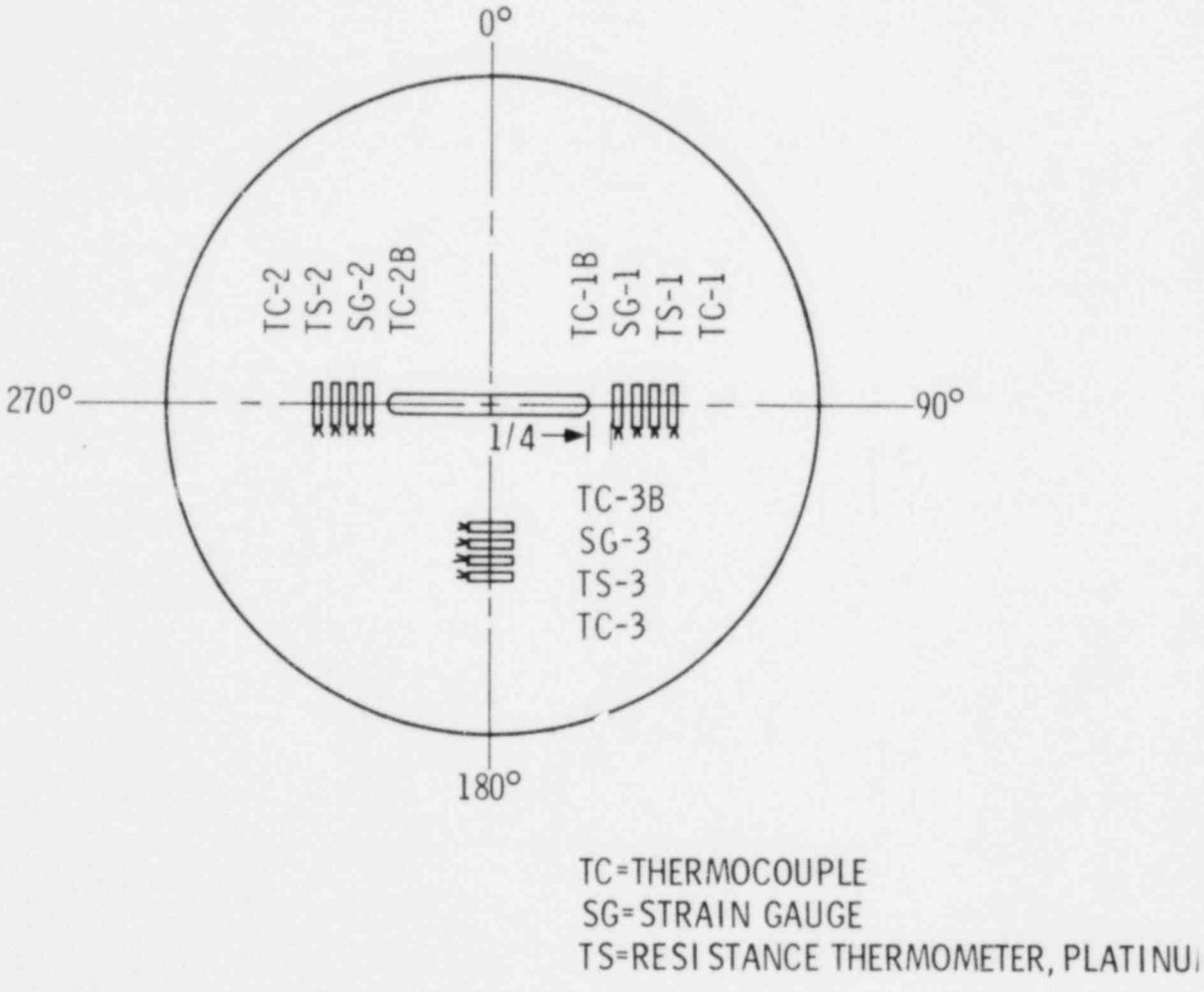

Figure 20. Steel Insert Strain Gauge and Thermocouple Instrumentation Schematic for Test 2

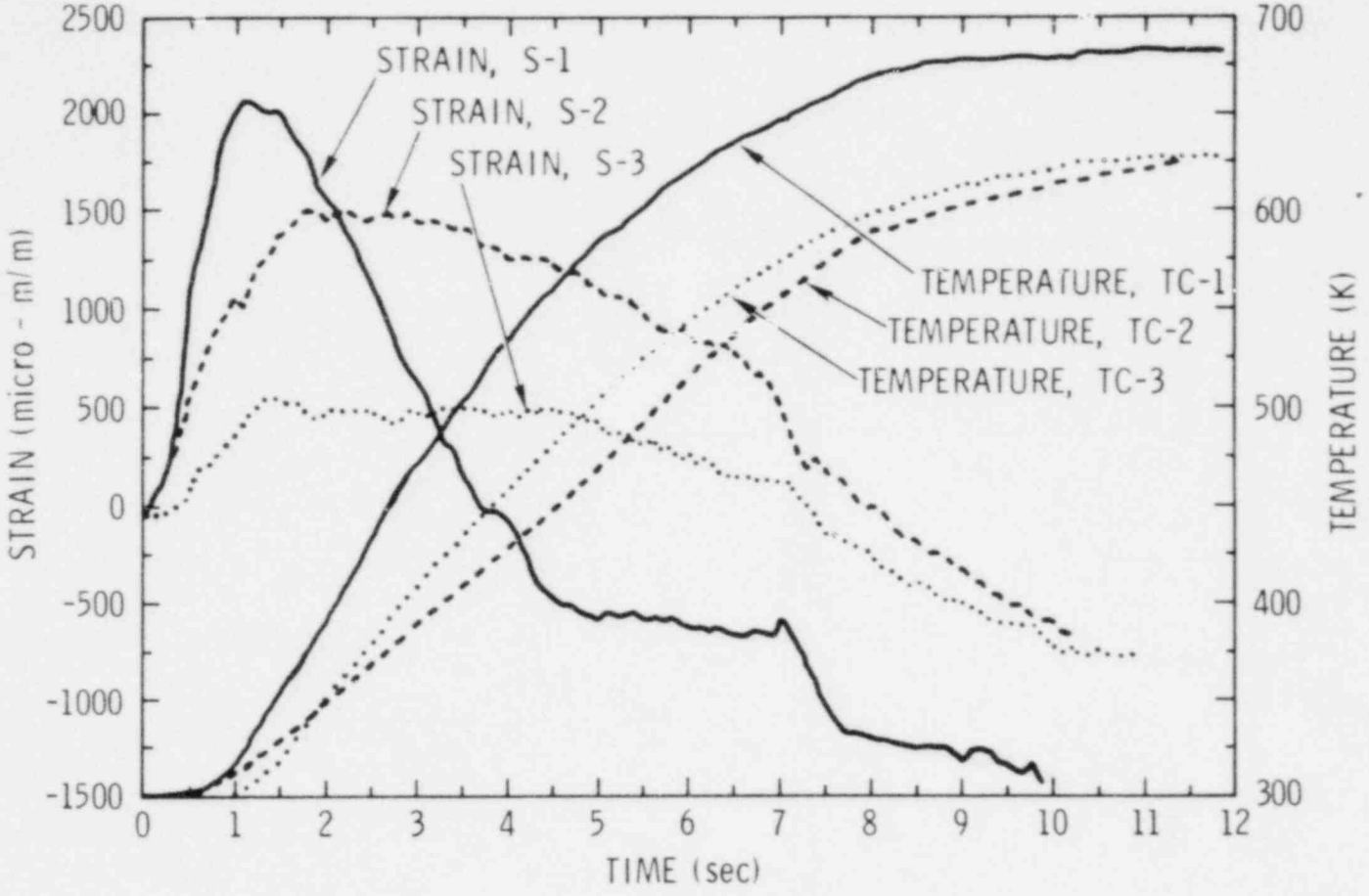

Figure 21. Steel Insert Strain and Temperature Response to Sodium Dump in Test 2

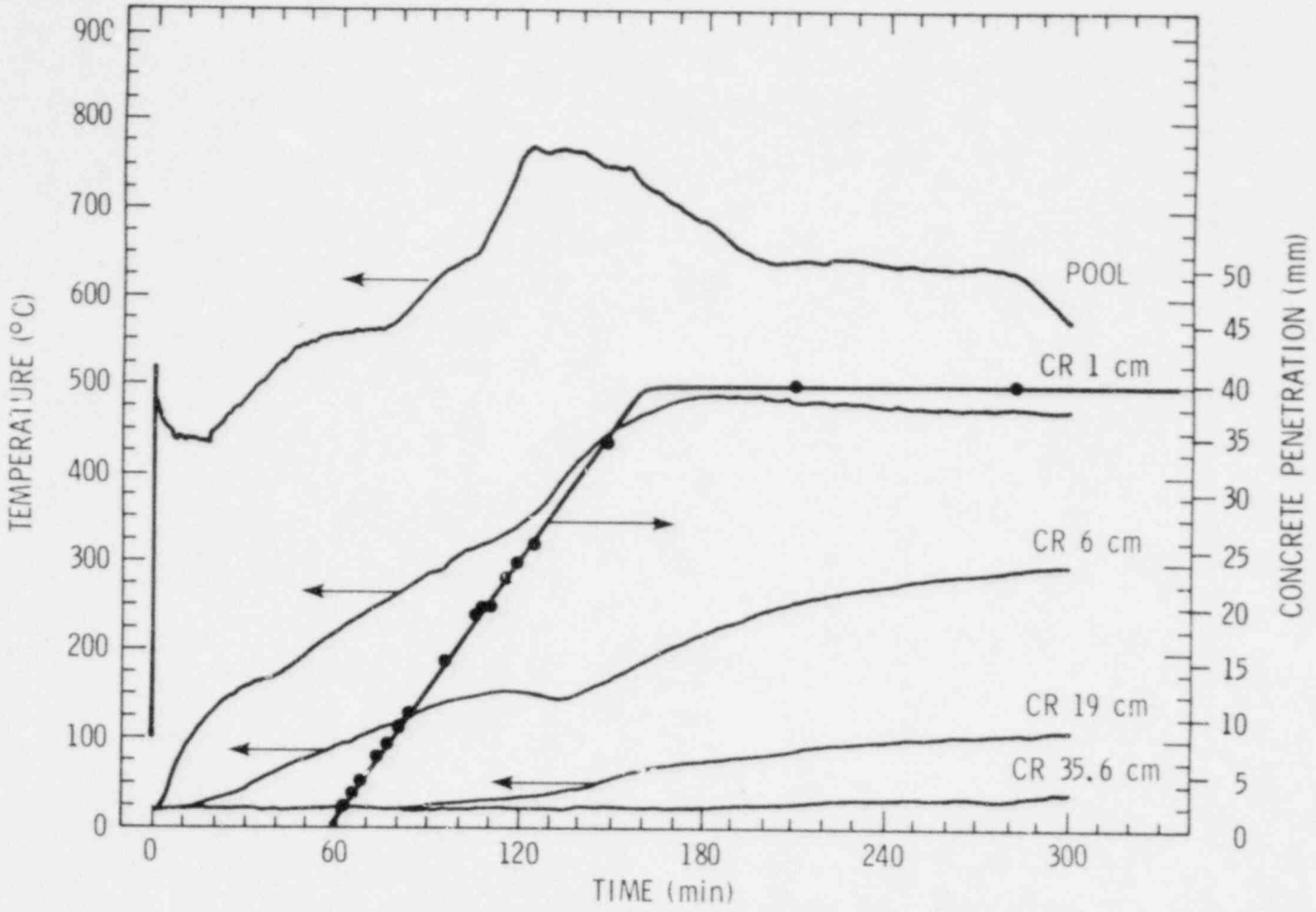

Figure 22. Penetration Data Added to Crucible Temperatures and Pool Temperature, Test 1

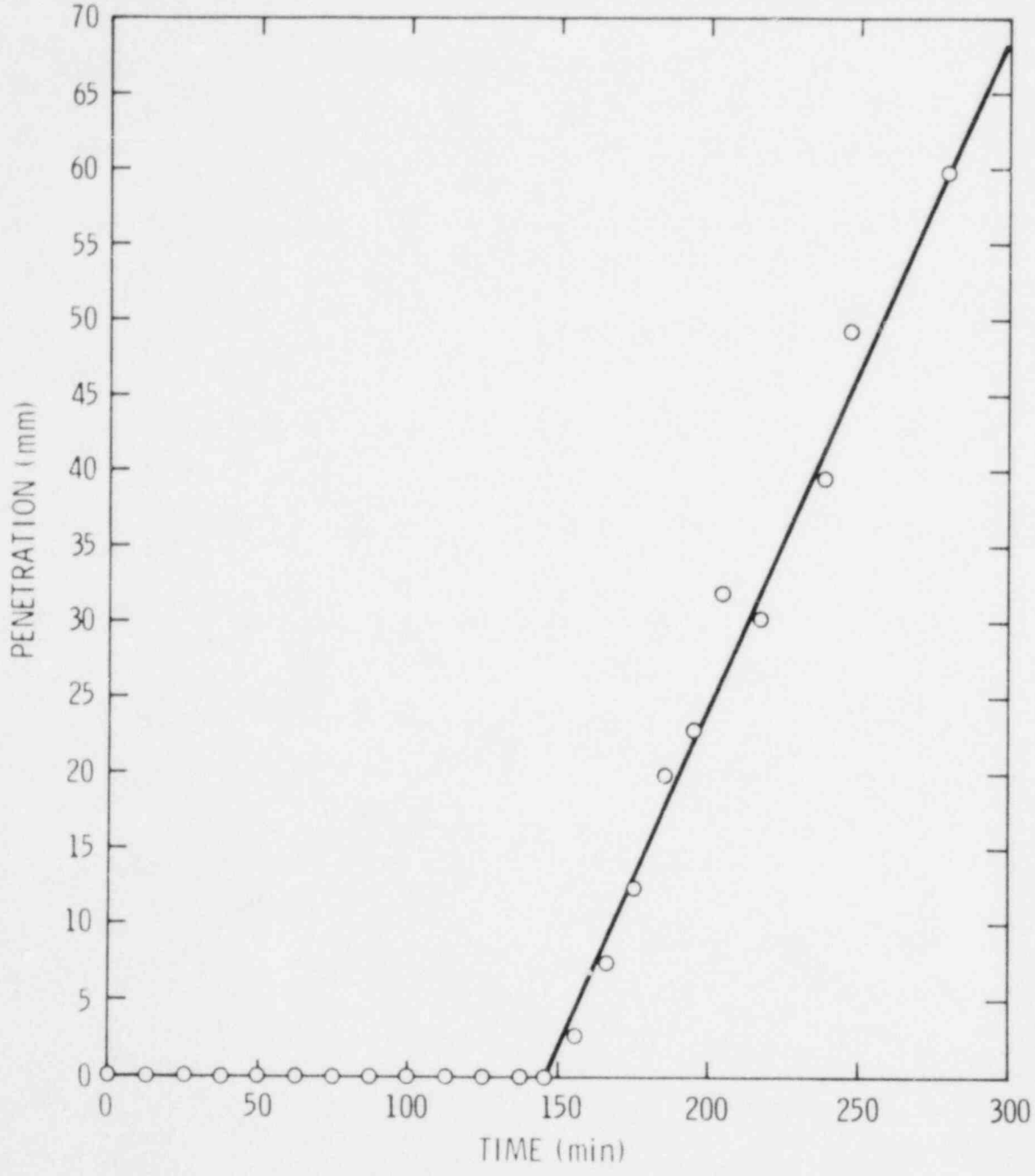

Figure 23. Ultrasonic Concrete Penetration Data for Test 3

and proceeded at a rate of about 0.5mm/min. The maximum penetration measured acoustically is about one-sixth of the total penetration found during posttest examination.

In both tests 1 and 3, the attack proceeded at a uniform rate. It therefore appears that spalling of the concrete does not contribute significantly to the observed erosion. If spalling occurred, discontinuities would be expected in the ultrasonic data as has been seen in some of our tests on limestone-aggregate concrete.

From the thermocouple traces shown in Figure 18, it is possible to estimate the rate of the reaction front movement into the firebricks and the concrete of test 3. An adjusted time zero was taken as that time at which the thermocouple on top of the dense firebrick (between the insert bottom plate and the firebrick) experienced its first excursion. This point in time is taken to be that time when sodium hydroxide saturation has taken place and firebrick attack by sodium hydroxide begins. (See section on Chemical Phenomenology.) From the adjusted time zero to the near vertical trace on the "middle" thermocouple gives a measure of the time necessary for the reaction front to traverse the dense firebrick (7.6 cm thick). Figure 24 shows the reaction front penetration rate developed from the above procedure. The last data point in Figure 24 was derived from posttest examination.

The results on concrete penetration by the two techniques (ultrasonics and thermocouples) agree fairly well when it is taken into account that the ultrasonics recorded only concrete penetration--not concrete plus firebrick penetration. The dash line in Figure 24 is the ultrasonic data with the firebrick penetration added and the time base adjusted.

Chemical Phenomenology

The detailed posttest chemical analyses of the reaction products from tests 1 and 3 are used to help construct a chemical reaction scenario for the molten sodium-basalt concrete interaction.

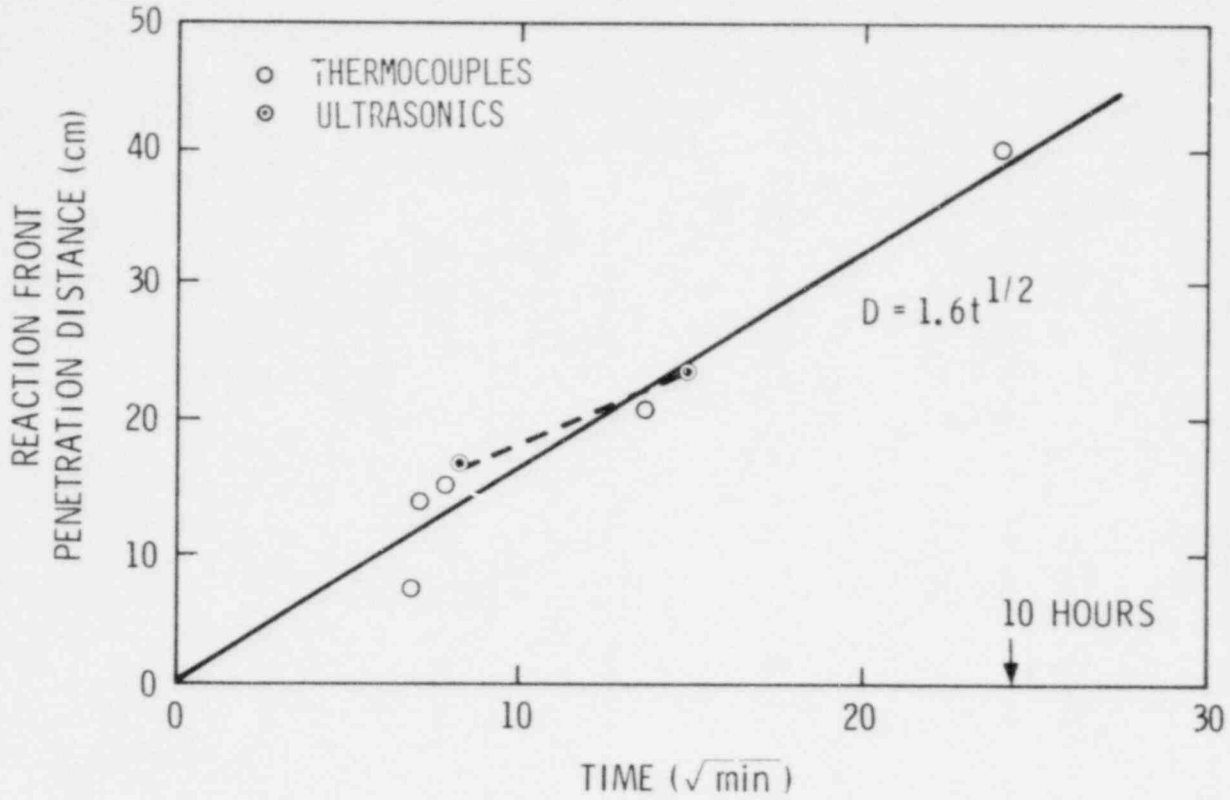

Figure 24. Penetration of the Sodium Reaction Front into the Firebrick and Concrete of Test 3

The initial chemical response of the concrete, or the firebrick, is the migration of water from the heated concrete volume being driven in part down the thermal gradient toward the exterior crucible surfaces. A significant portion of the water (possibly more than half) proceeds down a concentration gradient to the sodium-concrete interface where the water is consumed by a reaction with sodium. At the initial temperatures of these tests (T<973K) and with the creation of a predominately hydrogen gas atmosphere in the "tophat" volume, the reaction product is sodium hydroxide rather than sodium oxide, as shown in equation 3.

$$H_2O + Na \rightarrow NaOH + \frac{1}{2}H_2 \qquad (3)$$

The solubility of sodium hydroxide in sodium metal at these temperatures is large, as much as 10 - 20 mole percent.[7] Therefore, there is a delay while the sodium is being saturated with sodium hydroxide. The delay time can be long if the sodium metal pool is well stirred and has unrestricted access to the concrete surface. This was the case in test 1 where the pool heaters were needed to maintain the pool temperature for approximately 60 minutes into the test before additional chemically-generated heat became available. Conversely, this delay time will be short if the ratio of the sodium-concrete interface area to the sodium pool volume is large (i.e., shallow pools), or alternatively if the access of the sodium to the surface is restricted, as in tests 2 and 3. In these latter cases, only that sodium behind the insert (or in the firebrick pores) needs to be saturated.

Based on the flow rates of hydrogen gas for the first 60 minutes of test 1 and assuming that the hydrogen was generated according to equation 3, 12% of the sodium had reacted. This value is in good agreement with the saturation concentration of sodium hydroxide in sodium as reported by Shikhov.[7] Further calculations based on a

heat of reaction for equation 3 of 35kcal show that the chemically generated heat contributes about 27kW of power to the sodium pool and indicate that the heat losses from the crucible are on the order of 47kW.

When the sodium has become saturated with sodium hydroxide, a second liquid phase forms on the concrete surface. It is composed predominately of sodium hydroxide, but a sodium hydroxide which is saturated with respect to sodium metal. In a thermodynamic sense this new liquid phase is as reactive as sodium metal, being that it is in equilibrium with the metal. In a practical sense, it is more corrosive in that the concrete, or more precisely the silica and alumina components of the concrete, react with and dissolve into this new phase.

$$2NaOH + SiO_2 \rightarrow Na_2SiO_3 + H_2O \qquad (4)$$

$$2NaOH + Al_2O_3 \rightarrow NaAlO_2 + H_2O \qquad (5)$$

The water produced by these reactions is at a location where the chemical reactivity is equivalent to that of sodium metal, therefore this water reacts rapidly as in equation 3 to regenerate in part the NaOH. A truer measure of the chemically generated heat is given by a summation of these three equations.

$$H_2O + 2Na + SiO_2 \rightarrow Na_2SiO_3 + H_2 \qquad (4a)$$

$$H_2O + 2Na + Al_2O \rightarrow 2NaAlO_2 + H_2 \qquad (5a)$$

Remember that equations 4a and 5a are summation reactions and that the total process occurs only in the pressence of sodium hydroxide which is not only an intermediate reaction product but which is also a solvent in which the reactions proceed. Remember also that a sodium hydroxide phase exists only when the sodium metal is saturated, at least locally, with sodium hydroxide. Saturation of the sodium metal with sodium hydroxide is the crucial condition for concrete attack.

After the saturation condition has been met, a reaction front moves into the concrete. Its progress and character result from a delicate interplay of thermal and chemical gradients. To calculate the progress of that front requires more data than are presently available on 1) the thermal transport in concrete, 2) the chemical diffusion processes in concrete and in the reaction product, and 3) the rates and heats of the chemical reactions.

To illustrate this interplay, consider the evolution of hydrogen gas. In the initial stages of the sodium-concrete interaction. hydrogen gas is produced, as in equation (3), at the sodium-concrete interface and can bubble freely through the molten sodium pool. Later, when the reaction front has proceeded into the concrete, hydrogen gas is generated within a reaction product mass. The gas transport is more restricted and a portion of the gas ends up as sodium hydride, test 3. Within the reacting mass, local hydrogen gas pressures in excess of one atmosphere are presumed to be generated so that the sodium hydride may be formed.

The chemical character of the reaction front is not completely defined at the present time. The post-test analyses on test three indicate that the advanced portion of the reaction front has a large concentration of sodium hydroxide with water soluble sodium silicates and sodium aluminates. Behind this is a dark material containing sodium meta-silicate and sodium aluminate together with various amounts of sodium hydroxide, sodium oxide and sodium hydride. Exactly where in the reaction front the heat producing reactions occur is still a matter of conjecture; although if the spatial thickness of the reaction front is small, the location may be unimportant.

Conclusions

The conclusions drawn from the results of the three tests on basalt concrete may be summarized as follows:

1. The reactions between molten sodium and basalt concrete and between molten sodium and siliceous firebrick appear to continue as long as reactants are available--at least in the size scale and temperatures of these tests.
2. The phase that attacks the concrete and firebrick is sodium hydroxide for temperatures less than approximately 973K.
3. Reaction products build-up can cause liner deformation and concrete cracking.
4. Once the concrete has cracked:
   a. Sodium will preferentially attack the concrete along the cracks because of the increased surface area for water release.
   b. Hydrogen gas can escape from the reaction area and accumulate elsewhere.
5. Siliceous firebricks do not act as a barrier to the attack on basalt concrete by molten sodium.
6. The basalt concrete did not spall under the conditions of these tests.
7. The steel insert flaws did not propagate due to the initial sodium spill nor the subsequent reaction product build-up.

Future Work

The work on basalt concrete will continue on both large-scale and separate effects testing. An additional large-scale test is needed to answer the question as to whether the concrete water release rate is a linear or a parabolic function. Experimental evidence to date indicates a linear rate. A test similar to test 1 but with twice the sodium pool depth would settle the question. If the rate is linear, the delay time until sodium hydroxide saturation will be twice as long as in test 1. If the rate is parabolic, the delay time until saturation will be four times as long as in test 1.

Separate effects tests will look at the parameters of initial sodium pool depth and pool temperature. The chemical tests will continue the investigation of the $Na:H_2O:SiO_2$ phase diagram. Heat transfer tests will provide statistical information on the thermophysical properties of basalt concrete.

Appendix A

Water Release from Concrete and Firebrick During Heating

Some of the reactions that release heat as a result of the contact of molten sodium with concrete involve the water released from the concrete reacting with sodium:

$$Na + H_2O \rightarrow NaOH + \frac{1}{2}H_2 \qquad (A1)$$

$$2Na + H_2O \rightarrow Na_2O + H_2 \qquad (A2)$$

Therefore the amount of water given off by concrete is important in analysing sodium-concrete interactions.

Samples of basalt concrete were obtained for water release experiments. The concrete was made from "fine" aggregate (9.5MM mesh) per ASTM C-33 and ACI-613-54. The mixing ratio is given in Table A.

TABLE A

Basalt Concrete Mixing Rations

	Kilograms
Cement	42.6
Water	20.4
Sand	104.3
Aggregate	93.0
AEA*	0.02
WRA**	0.03

* Air entrainment agent

**Water reducing agent

Samples were taken and stored at 100% relative humidity for compression tests at 7, 28, and 90 days. These results are shown in Table B.

TABLE B

Water Release	Samples Strength
7 days	22.5 MPa
28	26.1
90	33.9

The samples were measured and weighed and then heated to some selected temperature. The samples were maintained at temperature until repeated weight measurements showed no significant weight change. The temperature was then raised to the next selected value.

Weight loss from concrete as a function of temperature consists of three distinct events: 1) loss of evaporable water (300K to 523K), 2) loss of chemically bound water (673K to 823K) and 3) loss of carbon dioxide (823K to 1073K).

Data for three basalt concrete samples are given in Figures A1 and A2. Two samples were measured in this study, the third set of data is from reference 6.

In order to gain some insight into the amount of water contributed by the firebricks and the mortar, samples of these materials were dried. These results are given in Table C.

The weight of the dense firebrick used in test 3 was 60.08kg and of the insulating firebrick 11.17kg. The weight of the mortar used was 11.5kg. The mortar weight was obtained by close accounting during layup of the firebricks in the crucible. From these total weights and the information in Table C it can be calculated that the firebricks and mortar of test 3 contained 1.04kg of water to contribute to the reaction with sodium.

As a matter of general interest, one each of the dense firebrick and insulating firebrick were immersed in water for 31 days. The insulating firebrick increased in weight by 244%, the dense firebrick by 7.9%.

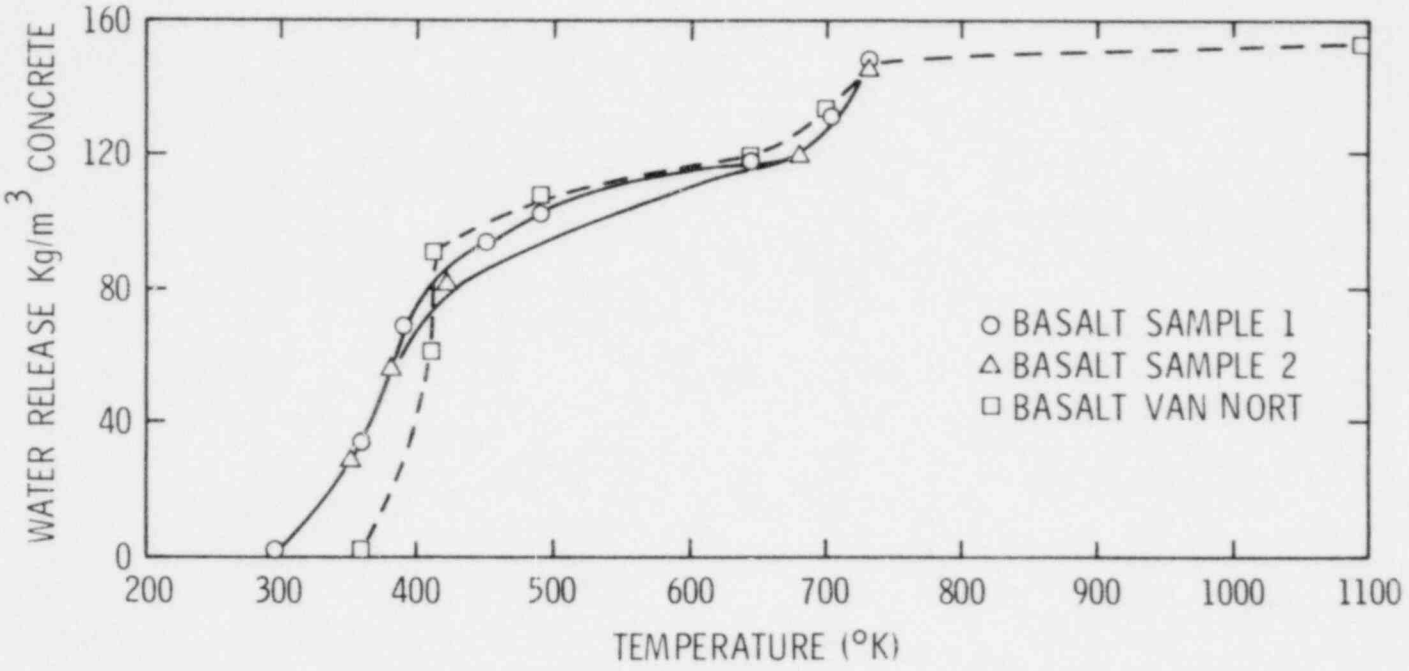

Figure A1. Water Release from Basalt Concrete on Heating

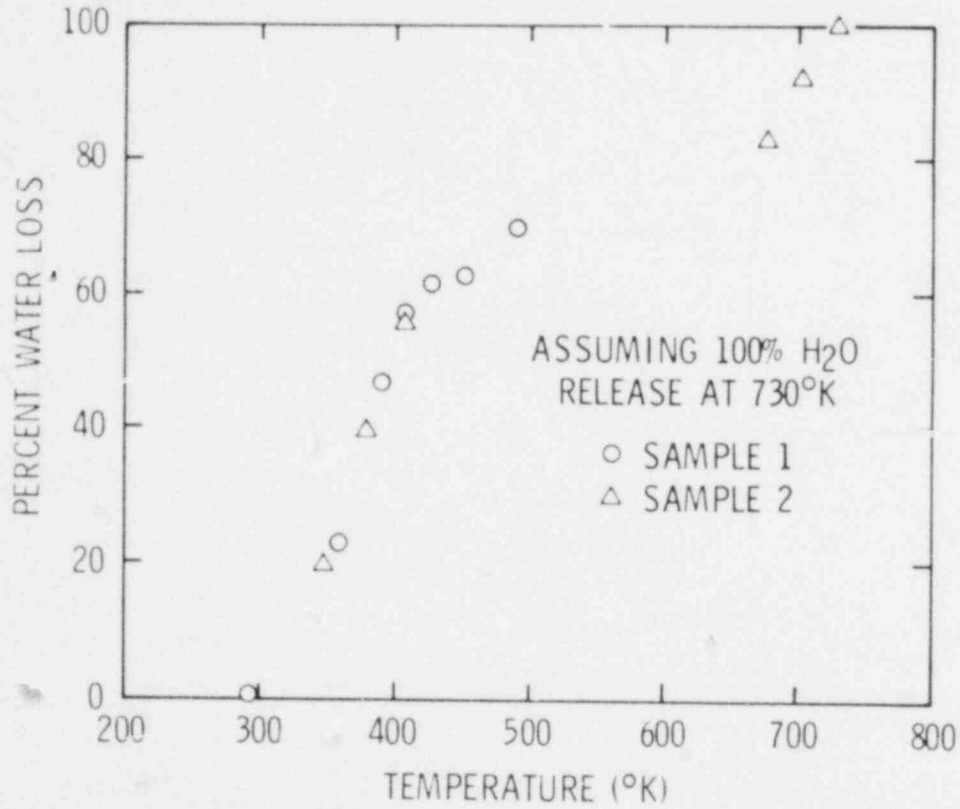

Figure A2. Percentage of Total Water Released from Basalt Concrete on Heating

TABLE C

Firebrick and Mortar Water Loss on Drying

Time Hours	Temperature K	Weight gm	Water Loss gm	%Weight Loss
		"Morex" Firebrick		
0	295	4291.5	-	-
24	500	4282.0	9.5	0.22
96	500	4276.8	14.7	0.34
		"G-20" Insulating Firebrick		
0	295	797.7	-	-
24	500	796.7	1.0	0.13
96	500	792.9	4.8	0.60
		"Troweleze" Mortar (air dry)		
0	295	36.93	-	-
28	295	33.54	3.4	9.2
52	295	32.98	3.95	10.7
100	295	31.91	4.02	10.9
244	295	30.96	5.97	16.2
		"Troweleze" Mortar (oven dry)		
0	295	36.77	-	-
28	500	28.35	8.4	22.8
244	500	28.35	8.4	22.8

Appendix B

Strain Gauge Investigation

In order to use the nickel-chromium strain gauges on the back side of the crucible cavity steel insert, it was necessary to determine how the gauges respond to a temperature increase of 55K/s. The nominal composition of the alloy is 0.74 Ni, 0.20 Cr, 0.03 Fe and 0.03 Cu. The commercial designation is AILTech model SG125-09F-4.

The experimental apparatus consisted of 25.4 cm long steel tube with a 2.54 cm O.D. and a 0.089 cm wall. Heating was achieved with a 236 watt/cm infra-red lamp mounted coaxially in the center of the tube. Intrinsic thermocouples and the strain gauge were mounted on the outside of the tube. Power to the heater was regulated so that a temperature rise of 55K/s was achieved on the outer surface of the tube. Comparing the static temperature characteristic of the strain gauge to the output observed at the 55K/sec change revealed that the output was in error by a maximum of 360$\mu\varepsilon$ during the thermal transient calibration. Each division on the strain ordinant of Figure 21 is 250$\mu\varepsilon$. An analytical determination of the thermal stress in the heated tube during the transient resulted in a maximum stress level of about 4.8 MPa.

Appendix C

Separate Effects Tests

Chemical

In the large-scale tests, many chemical reactions proceed simultaneously. Although a reaction scenario can be deduced, the individual reaction rates are difficult to estimate, let alone quantify. As a result, smaller-scale experiments in which individual reactions may be studied are necessary.

Two reactions have been studied thus far--the reaction of water vapor with sodium and the reaction of sodium hydroxide with silica.

Water driven from the concrete by hot, molten sodium is presumed to reach the sodium-concrete interface as a gas. The reaction of water vapor with sodium can lead to alternative reaction products (equations C1-C4) depending upon temperature, hydrogen pressure and the relative kinetics of the various reactions.

$$Na + H_2O \rightarrow (NaOH) + \tfrac{1}{2}H_2 \qquad (C1)$$

$$2Na + H_2O \rightarrow (NaOH) + (NaH) \qquad (C2)$$

$$2Na + H_2O \rightarrow (Na_2O) + H_2 \qquad (C3)$$

$$3Na + H_2O \rightarrow (Na_2O) + (NaH) \qquad (C4)$$

A major question is the disposition of the hydrogen; whether it is given off as the gas or dissolved in the sodium as in equations C2 and C4.

Experiments have been conducted in which water was flashed into an evacuated chamber containing molten sodium and the resulting gas pressure was monitored. If equations C2 and C4 are predominant, then little gas pressure would be observed. If equations C1 or C3 are predominant, the gas pressure should rise rapidly. Experimentally a

rapid gas pressure rise was observed. Pressures exceeding one atmosphere were reached within one minute. The gas pressure then gradually fell to a lower equilibrium value over a period of 1 to 4 hours. The interpretation is that reactions yielding hydrogen gas are favored by kinetics but that a slower dissolution of hydrogen occurs as a result of the hydrogen overpressure.

$$Na + H \rightarrow (NaH) \qquad (C5)$$

Data has been published[7] which indicate that at 673K to 873K sodium hydroxide is the phase which coexists with sodium metal. Thus equation C1 is taken as the predominant reaction, occurring whenever the hydrogen gas can escape--as in test 1. However, if the movement of the hydrogen gas is inhibited so that locally high overpressures of hydrogen can occur or so that much longer contact times are maintained, then significant quantities of hydrogen may be retained in the sodium.

The reaction of sodium hydroxide with silica can give various silicates. Although the meta-silicate (Na_2SiO_3) was found to be a major component of test 1-3, the desilicate ($Na_2Si_3O_5$) has been postulated to be a product at higher temperatures. Very little data on reaction rates, reaction products and melt compositions are known for compositions between NaOH and SiO_2. A series of experiments has been started to identify which silicates are formed as composition (NaOH:SiO_2 ratios) and temperature are varied.

The work completed thus far has considered NaOH rich compositions with NaOH:SiO_2 ratios greater than two. It has shown that mixtures of the meta-silicate and orthosilicate (Na_4SiO_4) are formed at temperatures of 773K and lower. Compositions with NaOH:SiO_2 ratios of less than two are currently being investigated.

Physical

Physical separate effects tests have not begun on basalt concrete. The facility has been constructed and several tests run on limestone

concretes. The tests will involve parameter variations on initial sodium temperature, initial sodium pool depth, etc.

Heat Transfer

Heat transfer tests were run on basalt concrete samples cast from the same batch as the crucible of test 1. The samples were 15.2 cm in diameter by 10.2 cm long. Thermocouples were cast into the samples at various distances from their flat faces. The samples were placed with their flat faces together with a flat heater in between. This arrangement provides for nearly one-dimensional heat flow in the samples. Since the heater is thin compared to its area, the assumption can be made that the power generated within the heater is equally partitioned between the two samples.

Power to the heater was provided by a computer controlled power supply in order to produce a sine-wave temperature variation in the heater--and consequently also at the sample faces. Having established a sinusoidal temperature wave at the sample surface, it is possible to measure the thermal diffusivity of the concrete by either the amplitude decrement or the phase difference techniques.[8]

$$\alpha = \frac{\pi f L^2}{(\ln q)^2} = \frac{\pi f L^2}{\phi^2} \qquad \text{(C6)}$$

where

α = thermal diffusivity

f = oscillation frequency

L = distance between two measuring points

q = amplitude ratio between two measuring points

ϕ = phase difference between two measuring points

The amplitude ratio method is reported to give better results than the phase difference method.

Figure C1 is a plot of the surface temperature sine wave and a thermocouple located 0.00456m into the concrete sample. The amplitude

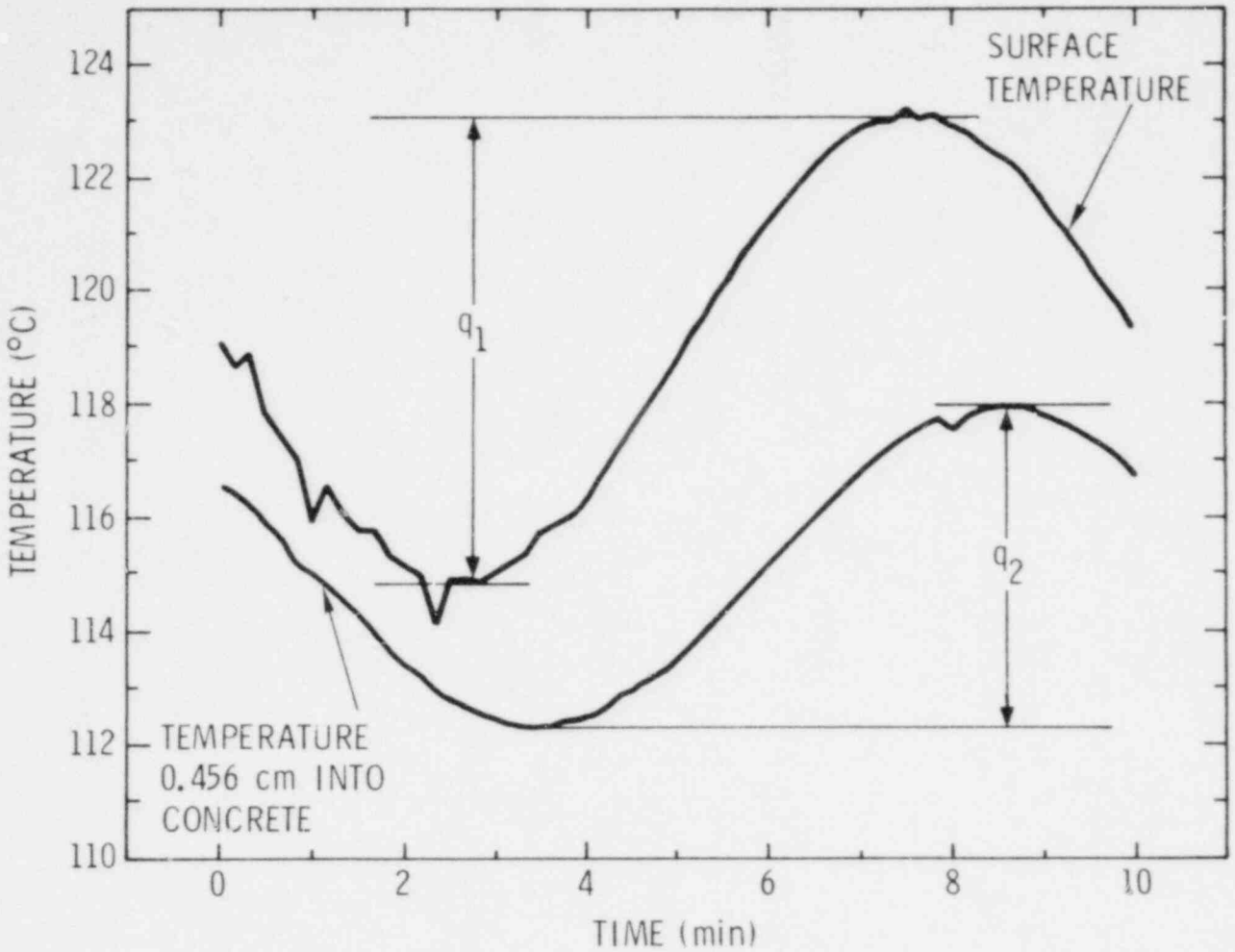

Figure C1. Sinusoidal Temperature in Basalt Concrete
$q_1/q_2 = 1.45$

decrement is 1.45--yielding a thermal diffusivity of 0.0028m^2/hr. This value is within 5% of the values reported in the literature.

Besides measuring thermal diffusivity, another reason for conducting these tests is to develop a technique for checking thermocouple locations in the large-scale crucibles. The thermocouples are securely positioned in the forms before the crucibles are cast. However, there is always the possibility that the weight of the concrete or the vibratory cement settling tool may shift a thermocouple's location. A large, flat heater can be placed on the bottom of the crucible cavity. The heater would subject the crucible bottom to a sinusoidal temperature wave. The amplitude and relative positions of the thermocouple outputs would provide a check on thermocouple position. If a thermocouple was out of position, its position could be calculated assuming that the thermal diffusivity of the concrete is reasonably well known.

References

1. H. J. Sutherland and L. A. Kent, "Erosion Rate Measurement Using an Acoustic Technique," Rev., Sci., Instr., 48, 1010, (1977).
2. H. J. Sutherland and L. A. Kent, "Acoustic Wave Measurements in Reactor-Grade Concretes," Trans. 4th SMIRT Conf. E, 6/5 (1977).
3. H. J. Sutherland, "Measurements of the Penetration of Molten Core Materials into Concrete Using an Acoustic Technique," Proc. Annual Post-Accident Heat Removal 'Information Exchange,' 425, (1977).
4. Central Premix Cement Co., Terminal Annex Box 3366, Spokane, Wa. 99220.
5. Private communication, D. E. Simpson, Hanford Engr. Devel. Lab., Dec. 15, 1977.
6. Private communication, P. S. VanNort, PMC, to R. S. Boyed, NRC.
7. B. A. Shikhov, Russian J. Inorgan. Chem., Vol 12, (4), pp. 545-548.
8. Y. S. Touloukian, R. W. Powell, C. Y. Ho, and M. C. Nicolaou, "Thermophysical Properties of Matter Vol. 10, Thermal Diffusivity," IFI/Plenum, N. Y., 1973, p. 29a.

DISTRIBUTION:

US Nuclear Regulatory Commission
(310 copier for R-7)
Division of Document Control
Distribution Services Branch
7920 Norfolk Avenue
Bethesda, MD 20014

US Nuclear Regulatory Commission (4)
Division of Reactor Safety Research
Office of Nuclear Regulatory Research
Washington, DC 20555
Attn: C. N. Kelber, Assistant Director
Advanced Reactor Safety Research
M. Silberberg, Chief
Experimental Fast Reactor Safety Br.
R. W. Wright
Experimental Fast Reactor Safety Br.
R. T. Curtis
Advanced Reactor Safety Research

US Department of Energy (2)
Office of Nuclear Safety Coordination
Washington, DC 20545
Attn: R. W. Barber
T. E. McSpadden

US Department of Energy (2)
Albuquerque Operations Office
P. O. Box 5400
Albuquerque, NM 87185
Attn: J. R. Roeder, Director
Operational Safety Div.
D. K. Nowlin, Director
Special Programs Div.
For: C. B. Quinn
D. Plymale

University of Michigan
Nuclear Engineering Department
Ann Arbor, MI 48104

General Electric Corporation (5)
310 De Guigne Drive
Sunnyvale, CA 94086
Attn: J. O. Bradfute, Mgr., Dynamics and Safety
A. S. Gibson, Mgr., Product Engineering
E. L. Glueckler, Mgr., Reactor Studies
J. E. Mott, Sr. Engineer, Dynamics & Safety
M. I. Temme, Mgr., Safety Analysis

W. E. Nyer
P. O. Box 1845
Idaho Falls, ID 83401

DISTRIBUTION (Cont):

Projekt Schneller Brueter (2)
Kern for chungszentrum Karlsruhe GMBH
Post fach 3640
D75 Karlsruhe
West Germany
Attn: Dr. Kessler
Dr. Heusner

Institut de Protection (3)
Et de Surete Nucleaire
CEN Fontenay-aux-Roses
B. P. 6
92260 Fontenay-aux-Roses
France
Attn: M. Tanguy
M. Schmitt
M. Cogne

Safety Studies Laboratory (2)
Commissariat a L'Energie Atomique
Centre d'Etudes Nucleaires de Cadarache
B. P. 1, 1311 Saint-Paul-les-Durance
Bouches-Du-Rhone
France
Attn: M. Bailey
M. Meyer Heine

H. J. Teague (3)
UKAEA
Safety and Reliability Directorate
Wigshaw Lane
Culcheth
Warrington, WA8 4NE
England

R. G. Bellamy
Reactor Fuels Group
AERE Harwell
Oxfordshire OXII ORA
England

J. G. Tyror, Head
Reactor Development Division
UKAEA-Atomic Energy Establishment
Winfrich, Dorchester
Dorset, England

Power Reactor & Nuclear Fuel (2)
Development Corporation (PNC)
Fast Breeder Reactor Development Project (FBR)
9-13, 1-Chome, Akasaka
Minato-Ku, Tokyo
Japan
Attn: Dr. Mochizuki
Dr. Watanabe

DISTRIBUTION (Cont):

1100 C. D. Broyles
Attn: G. E. Hansche, 1120
G. L. Ogle, 1125
H. E. Viney, 1130
J. H. Davis, 1136
1253 G. W. Gobeli
Attn: K. T. Stalker, 1253
1537 N. R. Keltner
Attn: T. Y. Chu, 1537
1537 R. U. Acton
1537 L. A. Kent
1550 F. W. Neilson
Attn: O. J. Burchett, 1552
J. H. Gieske, 1552
2150 T. L. Workman
3434 B. N. Yates
4231 J. H. Renken
Attn: J. A. Halbleib, 4231
P. J. McDaniel, 4231
J. E. Morel, 4231
4400 A. W. Snyder
4410 D. J. McCloskey
4420 J. V. Walker
4422 R. L. Coats
4422 J. E. Gronager
4422 J. B. Rivard
4423 J. E. Powell
4423 R. A. Beyerlein
4423 J. G. Kelly
4423 D. A. McArthur
4423 K. O. Reil
4423 H. L. Scott
4423 W. H. Sullivan
4423 S. A. Wright
4424 P. S. Pickard
4424 J. T. Hitchcock
4424 D. H. Worledge
4425 W. M. Breitung
4425 W. J. Camp
4425 R. W. Ostensen
4425 J. L. Portugal
4425 D. C. Williams
4425 M. F. Young
4425 R. J. Lipinski
4442 W. A. Von Riesemann
4450 J. A. Reuscher
4451 T. R. Schmidt
4452 L. D. Posey
5500 O. E. Jones
Attn: D. H. Hayes, 5510
D. F. McVey, 5511
D. O. Lee, 5511
R. D. Boyd, 5511
H. C. Hardee, 5512
5530 W. Herrmann
Attn: D. A. Benson, 5534
5534 J. E. Smaardyk
5800 R. S. Claassen

DISTRIBUTION (Cont):

5820 R. E. Whan
5822 N. E. Brown
5830 M. J. Davis
Attn: R. W. Rohde, 5832
J. L. Ledman, 5833
5831 N. J. Magnani
5831 D. A. Powers
5835 C. H. Karnes
5846 R. A. Sallach
8266 E. A. Aas
3141 T. L. Werner (5)
3151 W. L. Garner (3)
For DOE/TIC (Unlimited Release)
3172-3 R. P. Campbell, (25)
For NRC distribution to NTIS